UCGE Reports
Number 20137

Department of Geomatics Engineering

Spectral Analysis of Gravity Field Data and Errors in view of Sub-Decimetre Geoid Determination in Canada

(URL: http://www.geomatics.ucalgary.ca/GradTheses.html)

by

Olugbenga Esan

May 2000

THE UNIVERSITY OF CALGARY

Spectral Analysis of Gravity Field Data and Errors in view of Sub-Decimeter Geoid Determination in Canada

by

Olugbenga Esan

A THESIS
SUBMITTED TO THE FACULTY OF GRADUATE STUDIES IN
PARTIAL FUFILLMENT OF THE REQUIREMENTS FOR THE DEGREE
OF MASTER OF SCIENCE

DEPARTMENT OF GEOMATICS ENGINEERING
THE UNIVERSITY OF CALGARY
CALGARY, ALBERTA, CANADA

MAY, 2000

ABSTRACT

Recent developments in the modern geodetic, geophysics and oceanographic applications require a geoid with absolute accuracy of 10 centimetre or better and a relative accuracy of 1 part per million (ppm) of the inter-station distance. Gravity field data in Canada are spectrally analysed with the view of refining geoid estimation methods that will yield the above-mentioned accuracy requirements. The analysis is based on estimates of empirical covariance functions and degree variances derived from local gravity observations, a global geopotential model (EGM96), and topographic heights.

Numerical results for selected areas in mountainous, flat and marine areas of Canada show that the empirical signal and error covariance functions are non-uniform and they are highly correlated with the roughness of the topography. Gravity data and topographic heights with 1′ spatial resolution are required for 1 cm geoid in the mountainous areas while the same level of geoid accuracy can be achieved with 5′ data set in the flat areas. In addition, rigorous modelling of the topographic effects with actual topographic density values, as well as combination of the solution from the GM and Stokes's integral using gravity data in a cap size of 10°×10° is required for accurate geoid estimation.

PREFACE

This is an unaltered version of the author's Master of Science in Geomatics Engineering thesis of the same title. The Faculty of Graduate Studies accepted this thesis in May 2000.

The faculty supervisor for this work was Dr. M. G. Sideris. Other members of the examining committee were Dr. N. El-Sheimy and Dr. B.J. Maundy.

ACKNOWLEDGEMENTS

My gratitude goes to my distinguished supervisor, Dr. Michael G. Sideris, who despite his tight schedule has been very supportive. I am grateful for his encouragement and constructive criticism throughout the course of my graduate studies.

Special thanks to Dr. K. P. Schwarz and Dr. J. A. R. Blais for the beneficial discussion we had during the course of this research. I am also indebted to Mr. C. Kotsakis for his advice, as well as for providing me with some computer programs used for the research.

I also wish to thank Mrs. Madelyn Bradley at the international student center of the University of Calgary for her advice, which have been very useful. The advice and assistance received from my colleagues, as well as other staffs of the department are also acknowledged.

Financial support for this research has been provided by the Natural Sciences and Engineering Research Council of Canada, Geodetic Survey Division of NRCan, and NEOIDE Network of Centres of Excellence research grants to Dr. M. G. Sideris.

DEDICATION

I wish to dedicate this thesis to my dad, Mr. E. Oluwole Esan, who has just passed away, as well as to my mum Mrs. Florence Esan.

TABLE OF CONTENTS

LIST OF TABLES

LIST OF FIGURES

NOTATION

Δg	gravity anomaly
Δg_{GM}	gravity anomaly computed from a geopotential model
Δg_r	residual gravity anomaly
C	terrain correction
DEM	digital elevation model
N	gravimetric geoid undulation
N_{DEM}	topographic indirect effect of geoid undulation
N_{GM}	geoid undulation computed from a geopotential model
$N_{\Delta gr}$	geoid undulation computed from Stokes integration
G	Newton's gravitational constant
GM	geopotential model
EGM	earth geopotential model
R	mean earth's radius
ρ	topographic density
γ	normal gravity on ellipsoid
φ	latitude
λ	longitude
C_o	variance of the covariance function
$\chi_{1/2}$	correlation distance
$\Delta\varphi$	grid spacing in latitude direction

$\Delta\lambda$	grid spacing in longitude direction
Δx	grid spacing in X-direction
Δy	grid spacing in Y-direction
h	topographic height
S	Spherical Stokes kernel function
Std	standard deviation
Var	variance
rms	root mean square
PSD	power spectral density
GPS	global positioning system
ppm	part per million
$\mathbf{F}$, $\mathbf{F}^{-1}$	Fourier transform operator and its inverse
$\mathbf{H}$, $\mathbf{H}^{-1}$	Hankel transform operator and its inverse
FFT	fast Fourier transform
u, v	frequency in X and in Y direction
n, m	degree and order of harmonic expansion
n_{max}	maximum degree of harmonic expansion
$\bar{c}_{nm}, \bar{s}_{nm}$	fully normalized geopotential coefficients
$\bar{P}_{nm}$	fully normalized associated Legendre function
c_n^2	degree variance of the gravity anomaly
$ó_n^2$	degree variance of the anomalous potential

CHAPTER 1

INTRODUCTION AND RESEARCH BACKGROUND

1.1 BACKGROUND AND PROBLEM STATEMENT

The demand for a high precision geoid, which is required for modern geodetic, geophysics and oceanographic applications, has necessitated the need to refine the theory and practical computation methods of geoid estimation. The absolute geoid accuracy required for these modern applications are in the range of few centimetres, with a relative accuracy of 1 part per million (ppm) of the inter-station distance. Although some major developments have been made in precise geoid estimation, the current geoid prediction methods and data availability are still far from meeting these high accuracy requirements. Therefore, more improvements in the theory and practical methods of geoid determination are needed in order to obtain centimetre level geoid and at the same time increase the computation efficiency and data handling of the methods.

Improvement in practical geoid estimation can be achieved through a thorough examination of existing geoid estimation methods and optimal data combination techniques. Geoid undulations can be determined by various prediction techniques such as least squares collocation, input output system theory, spherical harmonic expansions, Stokes's integral solution, Molodensky's solution, or their combination. The advantage of the least squares collocation lies in its ability to accept heterogeneous data as input observations. The accuracy of the results relies on both the accuracy of the observations and the reliability of the signal and error covariance functions (Moritz, 1980; Tscherning, 1984). With a given geopotential model, geoid undulations can be computed from a spherical harmonic expansion. The solution from the geopotential model however contains only the long wavelength information of the gravity field (Pavlis, 1997; Rapp

and Pavlis, 1990; Rapp, et al., 1991; Sideris and Li, 1992), which is inadequate for the level of accuracy required for modern applications. Stokes's integral computes geoid undulations from gravity anomalies. The use of Stokes's integral theoretically requires gravity measurements on the whole earth surface and gravity anomalies reduced to the geoid. In practice, Stokes's integration is done with a limited spherical cap size instead of over the whole earth, as the formula requires. For gravity reduction, some assumptions on the topographic density are made in order to estimate the mass outside the geoid (Heiskanen and Moritz, 1967) and thus further errors are introduced into the solution.

Therefore, it becomes apparent that the refinement of geoid determination methods can be achieved through analysis of the properties of gravity field signals and errors in order to derive reliable a-priori information provided by the signal and error covariance functions, as well as through the use of optimal data combination techniques. In addition, data reductions through rigorous modelling of the effect of topographic masses and density variations especially in the mountainous areas, and minimization of data errors propagated into the estimated geoid are necessary in order to achieve the required geoid accuracy.

Two methods are used to extract important properties of gravity field signals and errors. Both the space domain method and frequency domain methods, which utilize the fast Fourier transform (FFT) algorithm, have been used extensively to study the properties of the gravity field signals. The two methods have their advantages and disadvantages. In recent times, the spectral (frequency domain) technique has been more popular due to its computational ease. The space domain method was used to estimate empirical covariance functions of gravity anomalies for selected areas in Canada by, e.g., Schwarz and Lachapelle (1980a, 1980b). The resulting empirical covariance functions were then modeled by modifying global covariance models (Heiskanen and Moritz, 1967; Tscherning and Rapp, 1984). Knudsen (1987) also used the space domain method to estimate and model auto-covariance function for gravity anomalies and geoid heights, as well as the cross-covariance function between the two quantities. Many other covariance

modelling studies have also been reported in the literature (Vassiliou and Schwarz, 1987; Jordan, 1972; Tscherning and Rapp, 1974).

Spectral techniques provide excellent means of extracting gravity field information contained in each of the gravity field data with the view of determining the contribution to the gravity spectrum of each data type (Sideris, 1987; Forsberg 1984, 1986; Kotsakis and Sideris, 1999). Analysis of the gravity field spectrum should involve critical examination of the spectral information from each data set and from a combination of geopotential model (GM), local gravity data and heights, which respectively provide long, medium and short wavelengths information of the gravity field. Such analysis would provide the necessary gravity field signal and error covariance or power spectral density (PSD) functions required for geoid prediction techniques. In addition, estimates of data sampling density derived from degree variances of the gravity signal would give a better picture of the data requirement for geoid estimation with sub-decimetre accuracy.

Both the space domain and frequency domain methods need to be critically examined to determine which method will be better in estimating the covariance functions for a local area. It will also be necessary to know how the two methods could be combined to achieve the best results in extracting spectral properties of the gravity field signals. In addition, estimated PSD functions and degree variances should be thoroughly exploited in various spectral bands to determine the geoid power contribution in various spectral bands, as well as to estimate the data resolution required for centimetre to decimetre level of geoid accuracy.

Investigation of the contribution to geoid undulations of the GM coefficients and errors using the EGM96 geopotential model, in combination with local gravity in Stokes's integral, would provide the means of optimally combining the two data types. Consequently, the effects of truncating the degree of the spherical harmonic expansion of the GM in favour of using larger cap size to evaluate Stokes's integral need to be

examined. In similar studies, an increased area of integration has been shown to improve the results for geoid estimates (Schwarz, 1984; Sjoberg, 1987). The limit to which the cap size should be increased is investigated in order to derive an optimal cap size for Stokes's integral solution.

Critical analysis of the signal information from the short wavelength part of the gravity field spectrum in which the topographic terrain corrections have a dominant role is required in order for the centimetre geoid to be achievable. Li and Sideris (1994) established that the discrepancy between the gravimetric geoid and GPS/levelling derived geoid is correlated with the roughness of the topography. Therefore, rigorous modelling of the effect of topography and density variations especially in the mountainous areas would provide information on the recoverable geoid power in the very high spectral band.

Rigorous formulas for terrain correction have been proposed and used (Sideris 1984, 1985, 1990; Li, 1993). The effect of using mass prism topographic model and line prism topographic model is also documented in Li (1993). In all these studies constant density values were used for the computation of the terrain effect even in the mountainous areas. The effect of terrain correction with actual topographic density values on the estimated geoid needs to be examined if the sub-decimetre geoid is to be achieved especially in areas with very rough topography.

The overall achievable accuracy of predicted geoid is limited by a number of error sources. Of more importance are those errors in the geopotential model (GM), local gravity anomalies Δg, and heights, which are propagated into the geoid results through the prediction formulas. Smaller errors due to datum biases, spherical approximation, and the mass of the atmosphere are not considered in this study; further details can be found in Heiskanen and Moritz (1967). Proper description of the behavior of data source errors are provided by suitable covariance function models. While the error covariance function from the GM can be easily derived from the error degree variances of the coefficients,

empirical error covariance models have to be derived for the gravity and height data that will represent the actual error behavior for the local area. Sideris and Schwarz (1986) documented error covariance models of gravity and height for areas located in the North American continent. In order to derive error models for gravity and heights that will actually represent the local area, models for areas with different topography should be derived separately, and the overall geoid error from the data errors should be estimated and modeled for individual areas. In addition, a thorough analysis of errors from each of the data sources and combination of the data would provide a good picture of internal geoid accuracy achievable with each data type and combination of the data types.

Therefore, it can be expected that spectral analysis of the gravity field data can provide the information required for refining geoid estimation methods in order to obtain geoid with a cm level of accuracy in a local area. Information contained in the spectrum of different data types would provide the geoid rms power from each of the data types and their combination. Such information will be useful in determining the optimal procedures for combining the different data for the geoid prediction methods.

Furthermore, a thorough analysis and rigorous modelling of the effect of topography and density variation especially in the mountainous areas would improve the short wavelength information of the geoid in these areas.

1.2 RESEARCH OBJECTIVES

The main task of this study is to investigate how the practical geoid determination methods could be refined especially in terms of data requirements to achieve geoid estimates with sub-decimetre level of accuracy. Both space domain and frequency domain methods will be used to estimate empirical covariance functions of gravity anomaly for areas with different topographic features in order to examine their

correlation with the topography, as well as to investigate the use of uniform covariance function for prediction by collocation. Spectral techniques will be used extensively to extract the properties of local gravity field signals in various wavelength bands using the EGM96, local gravity anomalies, topographic densities and heights. Models for the decay of the spectrum of the gravity data at various wavelength bands will be derived and the results compared to standard models. In addition, rigorous terrain correction formulas will be used with lateral density variations to investigate the effect of using a constant topographic density value for terrain corrections and geoid indirect effects computation especially for high mountainous areas.

The role of the GM using EGM96 and local gravity data in geoid estimation will be investigated. Maximum degree of spherical harmonic expansion of the GM coefficients in combination with cap size of the Stokes integral will be studied to determine the effect of truncating the harmonic series in favour of using more local gravity data.

More specifically, the overall objectives of this research will be achieved through the following tasks:

- Derive covariance and power spectral density (PSD) functions for the gravity field signals and errors for areas with different topography, possibly marine, flat and mountainous areas.
- Derive estimates of the gravity and height spacing required for a given level of accuracy for the geoid.
- Investigate the role of topographic density variations especially in mountainous areas.
- Investigate the role of the GM maximum degree of expansion, in conjunction with Stokes integral cap size containing the local gravity data.
- Derive models for geoid errors from gravity, heights and GM, as well as the combined geoid error separately for flat and mountainous areas.

1.3 METHODOLOGY

Available gravity, topographic heights and density data for Canada, as well as EGM96 coefficients will be analyzed to derive the covariance and PSD functions of the data sets. The estimated PSD and covariance functions are used to derive corresponding degree variances for the gravity data which are then used to estimate the required gravity data spacing for various levels of accuracy of geoid prediction in the centimetre to decimetre range. Covariance and PSD functions will be estimated for selected areas in the marine, flat and mountainous areas of Canada. The results of the spectral analysis for the different areas will then be compared to determine the average spectral properties of the gravity field in the marine, flat and mountainous areas of Canada. Furthermore, the effect of using actual topographic density values for terrain corrections in mountainous areas will be investigated for areas selected in the Rocky Mountains of western Canada. Analysis will be based on topographic density data with 30″×30″ resolution and a digital elevation model (DEM) with 3″×3″ resolution. The results of the terrain corrections and geoid indirect effects derived with actual topographic density values will be compared with those obtained with a constant topographic density value.

Reduced gravity anomalies with 5′×5′ resolution in a block size of about $15^{o}\times15^{o}$ and EGM96 coefficients will be used to study the effect of truncating the harmonic expansion of the GM model in favour of using more local gravity in a cap size for Stokes's integration. Various values of maximum degree of spherical harmonic expansion will be used to estimate gravity anomalies from the reference model and subsequently used to derive various reduced gravity anomalies. For each set of estimated reduced gravity anomalies, the corresponding geoid undulation is estimated using Stokes's integral with varying cap size. The total geoid estimated for a given cap size and harmonic degree of expansion is then compared to geoid undulations derived from GPS/levelling benchmarks located within the area of analysis. In addition, the spectrum of the GM and local gravity data will be analyzed to determine better procedures for combining the GM coefficients with local gravity data.

Gravity data error covariance and PSD functions will be derived by modelling the differences between actual measurement and predicted observations for selected areas in flat and mountainous areas. The derived gravity error covariance models will be used to determine the magnitude of propagated geoid undulation errors for the flat and mountainous areas. An attempt will be made to compare internal propagated errors with external geoid errors derived from GPS/levelling benchmarks in the flat and rocky test areas.

1.4 THESIS OUTLINE

The thesis consists of seven chapters. The content of the next six chapters is summarized below.

Chapter 2 outlines the methodology and equations for conventional geoid estimation. The results of varying cap size in Stokes's integral and the maximum degree of spherical harmonic expansion for the GM coefficients are presented. The effect of lateral density variations on terrain correction and estimated geoid is presented as well.

In chapter 3, the basic concept of covariance and PSD estimation is discussed and equations relating the two functions, as well as their relation to the degree variances, are presented.

Chapter 4 discusses the results of local gravity anomaly empirical covariance functions for areas selected across Canada in the mountainous, flat and marine test areas. A comparison is made between the covariance functions derived from the space domain method with actual gravity data and those from the frequency domain method using

gravity data on a grid. The effect of data griding on the estimated covariance estimates is also discussed.

The variation of the gravity field spectrum at very high frequencies is discussed in chapter 5. Numerical results for flat and mountainous test areas in Canada are presented. In addition, the gravity data sampling density required for a level of geoid accuracy in the decimetre to centimetre range is also presented.

In chapter 6, models for gravity and height data error covariance functions are discussed. Numerical results of geoid error covariance from these data errors are presented for flat and mountainous test areas. External geoid errors derived from comparison of GPS and levelling benchmarks within the area of analysis are estimated and the results are compared with the internally propagated geoid errors in flat and mountainous areas to examine their correlation with the topography.

Chapter 7 summarizes the results of the whole study. Main conclusions and recommendations for geoid estimation and further research are also discussed.

CHAPTER 2

GEOID ESTIMATION WITH A GEOPOTENTIAL MODEL AND LOCAL GRAVITY DATA

This chapter discusses the role of the global geopotential model (GM), local gravity data and their combination in conventional geoid determination methods. In practice, the long wavelength geoid is usually estimated by a spherical harmonic expansion up to the maximum degree and order of the given GM. The contribution from the local gravity data is estimated by Stokes's integral with gravity anomalies in a given cap size which define the area of integration. The evaluation of Stokes's integral by FFT requires gravity anomalies on a regular grid. The interpolation of gravity anomalies is usually carried out with collocation, which requires reliable a priori information provide by signal and error covariance functions.

Section 2.1 of this chapter presents the conventional formulas for gravimetric geoid determination using the remove restore technique. Section 2.2 outlines the FFT formulas for evaluating the Stokes and terrain correction convolution integrals. Analysis of results for selected areas in Canada is discussed in section 2.3. In section 2.4, the effect of lateral topographic density variations on terrain correction and estimated geoid in mountainous areas is discussed.

2.1 FORMULAS FOR GEOID COMPUTATION

The computation of the gravimetric geoid undulation is accomplished by combining solution from three sources; a global geopotential model (GM), local gravity anomalies Δg, and the topography represented by a Digital Elevation Model (DEM) using the remove-restore technique. Local gravity anomalies are first reduced by removing the effect of the topography and the long wavelength contribution from a reference field. The effect of the topography and global field are then restored in the final expression for the geoid undulation. The expression for the gravimetric geoid undulation could therefore be written as

$$N = N_{GM} + N_{\Delta g_r} + N_{DEM} \tag{2.1}$$

where N_{GM} is the geoid undulation implied by the geopotential model, $N_{\Delta g_r}$ is the contribution of reduced gravity anomalies, which is derived from Stokes's integration, and N_{DEM} is the indirect effect of the topography.

The contribution of the GM coefficients, N_{GM}, at a point is computed by spherical harmonic expansion series (Heiskanen and Moritz, 1967), and is given in spherical approximation on the geoid as

$$N_{GM} = R \sum_{n=2}^{n_{max}} \sum_{m=0}^{n} \left(\bar{c}_{nm} \cos m\lambda + \bar{s}_{nm} \sin m\lambda \right) \bar{P}_{nm}(\sin\varphi) \tag{2.2}$$

where R is the mean radius of the earth, $\bar{c}_{nm}$ and $\bar{s}_{nm}$ are the fully normalized harmonic coefficients of the anomalous potential, $\bar{P}_{nm}$ are the fully normalized associated Legendre functions, and n_{max} denotes the maximum degree and order of expansion of the GM geopotential solution.

The Stokes formula for computing the geoid undulations is given as

$$N_{\Delta g_r} = \frac{R}{4\pi\tilde{a}} \iint_{\sigma} \Delta g_r(\varphi,\lambda) S(\psi) d\sigma \qquad (2.3)$$

where σ denotes the sphere of integration, φ and λ are the geocentric latitude and longitude of the data point respectively, $\tilde{a}$ is the normal gravity, Δg_r is the residual gravity anomaly, which has been corrected for the effect of the topography and referenced to a GM, $S(\psi)$ is the Stokes function, and ψ denotes the spherical distance between the data point and the computation point. Since in real world applications the gravity data are only available in discrete point locations, the expression in (2.3) can be rewritten for gravity anomaly data given on the sphere (Haagmans et al, 1992; Li and Sideris, 1994) as

$$N_{\Delta g_r} = \frac{R}{4\pi\tilde{a}} \sum_{\varphi=\varphi_1}^{\varphi_B} \sum_{\lambda=\lambda_1}^{\lambda_L} \Delta g_r(\varphi,\lambda) S(\psi) \cos\Delta\varphi \Delta\lambda \qquad (2.4)$$

where $\Delta\varphi$ and $\Delta\lambda$ are the grid spacing in latitude and longitude direction respectively, L and B define the cap size and they represent the number of meridians and parallels in the block respectively. The Stokes kernel function $S(\psi)$, can be expressed as

$$S(\psi) = \frac{1}{\sin\frac{\psi}{2}} - 4 - 6\sin\frac{\psi}{2} + 10\sin^2\left(\frac{\psi}{2}\right) - \left[3 - 6\sin^2\left(\frac{\psi}{2}\right)\right] \text{in}\left[\sin\frac{\psi}{2} + \sin^2\left(\frac{\psi}{2}\right)\right] \tag{2.5}$$

where

$$\sin^2\left(\frac{\psi}{2}\right) = \sin^2\left(\frac{\varphi_p - \varphi}{2}\right) + \sin^2\left(\frac{\ddot{e}_p - \ddot{e}}{2}\right)\cos\varphi_p\cos\varphi \tag{2.6}$$

The term Δg_r in equation (2.4) according to Helmert's second condensation reduction is given as

$$\Delta g_r = \Delta g_{FA} + C + \delta_{\Delta g} - \Delta g_{GM} \tag{2.7}$$

where Δg_{FA} is the free air gravity anomaly corrected for the atmospheric attraction, C is the classical terrain correction, $\delta_{\Delta g}$ is the indirect effect on gravity which, being very small, is neglected in this study, and Δg_{GM} is the gravity anomaly computed in spherical approximation on the geoid by the spherical harmonic expansion formula

$$\ddot{A}g_{GM} = \tilde{a}\sum_{n=2}^{n_{max}}(n-1)\sum_{m=0}^{n}(\bar{c}_{nm}\cos m\ddot{e} + \bar{s}_{nm}\sin m\ddot{e})\bar{P}_{nm}(\sin\varphi) \tag{2.8}$$

The terrain correction C, can be expressed in planar earth approximation as

$$C(x_p, y_p, h_p) = -G\iint_E \int_{h_p}^{z} \frac{\rho(x, y, z)(h_p - z)}{s^3} dxdydz \qquad (2.9)$$

where $s = \left((x_p - x)^2 + (y_p - y)^2 + (h_p - z)^2\right)^{\frac{1}{2}}$, G is the Newton's gravitational constant, ρ is the topographic density, h is the topographic height, (x, y, z) represents the running point, (x_p, y_p, h_p) represents the computation point, and E represents the integration area.

The indirect effect of Helmert's condensation reduction on the geoid in planar approximation, considering the first two terms is given (Sideris, 1990) as

$$N_{DEM}(x_p, y_p) = \frac{\delta G}{\tilde{a}} \rho(x_p, y_p) h^2(x_p, y_p) - \frac{G}{6\tilde{a}} \iint_E \frac{\rho(x_p, y_p)[h^3(x, y) - h^3(x_p, y_p)]}{s^3} dxdy \qquad (2.10)$$

See Sideris (1990) and Li (1993) for the detailed expression of geoid topographic indirect effect and its evaluation via FFT. 1D-FFT formulas for evaluating equation (2.4) are presented in the next section. Further details on the evaluation of convolution integrals in physical geodesy by FFT techniques can be found in Schwarz et al. (1989), Sideris (1994), and Sideris and She (1994). It should be noted that in using the FFT formulas, data on grids are 100% zero padded, to minimize the effect of circular convolution.

2.2 THE SPHERICAL STOKE'S FORMULA

The 1D FFT technique allows for the evaluation of the discrete spherical Stokes integral without approximation (Sideris and She, 1994). The result of equation (2.4) on a certain parallel of latitude φ_l using data along parallels of latitude φ_j can be expressed as

$$N_{\Delta g_r}(\varphi_l, \lambda_k) = \frac{R}{4\pi\gamma} \sum_{j=1}^{L} \left[\sum_{i=0}^{B} \Delta g(\varphi_j, \lambda_i) \cos\varphi_j S(\varphi_j, \varphi_i, \lambda_k - \lambda_i) \Delta\lambda \right] \Delta\varphi \qquad (2.11)$$

Since the bracket in (2.11) contains a one-dimensional discrete convolution with respect to λ, i.e., along a parallel, the expression for its evaluation is given for the fixed parallel φ_l as

$$N_{\Delta g_r}(\varphi_l, \lambda_k) = \frac{R \Delta\varphi \Delta\lambda}{4\pi\gamma} \mathbf{F}^{-1} \left\{ \sum_{i=0}^{W} \mathbf{F}\{\Delta g(\varphi_j, \lambda_i) \cos\varphi_j\} \mathbf{F}\{S(\varphi_j, \varphi_i, \lambda_k)\} \right\} \qquad (2.12)$$

where $\mathbf{F}$ and $\mathbf{F}^{-1}$ denotes the 1D Fourier transform operator and its inverse, respectively. Detail discussion on the derivation of equation (2.12) from equation (2.3) can be found in Sideris and She (1994), and Haagmans et al. (1992). The expression in (2.12) yields the geoid undulation for all the points on one parallel. The major advantage of using the 1D FFT approach lies in its ability to give exactly the same result as those obtained by direct numerical integration.

2.3 FORMULAS FOR TERRAIN CORRECTION WITH MASS PRISM TOPOGRAPHIC MODEL

For a given topographic density and height data on a grid, equation (2.9) under the assumption of uniform density within a topographic mass model, can be written as

$$C(x_p, y_p) = G\sum_{n=0}^{N-1}\sum_{m=0}^{M-1}\rho(x,y)T(x,y) \tag{2.13}$$

where $T(x,y)$ is the kernel function given as, Li (1993):

$$T(x,y) = x*\ln(y+s) + y*\ln(x+s) - z*\arctan\left(\frac{x*y}{z\,s}\right) - z*\arctan\left(\frac{xy}{z\,s}\right)\Bigg|_{x_p-(x+\Delta x/2)}^{x_p-(x-\Delta x/2)}\Bigg|_{y_p-(y+\Delta y/2)}^{y_p-(y-\Delta y/2)}\Bigg|_{0}^{h_p-h} \tag{2.14}$$

In equation (2.14), Δx and Δy represent the grid spacing in the x and y directions respectively, and the distance kernel $s = [(x_p - x)^2 + (y_p - y)^2 + (h_p - z)^2]^{\frac{1}{2}}$. The derivation of equations (2.13) and (2.14), and evaluation by 2D FFT is discussed in detail in Li (1993, pp. 70 - 83). In this thesis, the estimation of all terrain correction is implemented by the program originally written by Yecai Li (1993); some modifications are made to the original program to suite the size and format of the input and output data.

Equations (2.1), (2.2) and (2.4) to constitute the set of formulas adopted in this study for the computation of the gravimetric geoid. Specifically, equation (2.2) is used to derive the geoid contribution with various values of the degree and order of spherical harmonic

expansion of the EGM96 while equation (2.4) is used to derive the geoid with various cap sizes. Reduced gravity anomalies are derived by using equation (2.7); the reference gravity anomalies are derived with various degree and order of spherical harmonic expansion of the EGM96 by using equation (2.8) while the terrain corrections are derived by using equation (2.9). The effect of change in the integration cap size on the geoid indirect topographic effects in equation (2.10) is very small and is ignored in this study.

2.4 ANALYSIS OF RESULTS FOR GM AND GRAVITY DATA COMBINATION

2.4.1 **Data Sets Used**

An area between latitudes 50.0471 and 65.0471, and longitudes -128.0471 and -113.0471 $(15^0 \times 15^0)$ located in the Alberta and British Columbia provinces is selected for analysis. Gravity data with $5' \times 5'$ grid spacing and $1' \times 1'$ DEM data provided by the Geodetic Survey Division are used. The data sets belong to the same sets of data used for computing GSD95 geoid model (Veronneau, 1996). The gravity anomaly and geoid undulation from the GM is computed using the software developed in the department of Geomatics Engineering, University of Calgary by Li Y. C. (1993). The EGM96 geopotential model, which is complete to degree and order 360, is also used as the reference field. Newly adjusted leveling data referenced to the Canadian Geodetic Datum (CGD28) and GPS data points in the selected area are use to derive geoid undulation with which the estimated gravimetric geoid is compared. Table 2.1 shows the statistics of the reduced gravity anomaly data and heights used for the analysis.

Table 2.1: Statistics of residual gravity anomalies and heights used for GM and local gravity data analysis

Height (m)			
Min	Max	Mean	Std.
-1.83	3747.03	885.23	611

Residual Gravity Anomalies (mGal)				
Degree of Expansion	Min	Max	Mean	Std.
30	-113.2	148.1	1.5	27.0
60	-123.2	149.6	0.6	26.4
90	-130.5	135.2	-0.1	25.2
120	-136.3	136.6	0.0	24.3
180	-127.1	141.9	0.0	23.0
240	-141.5	127.3	0.0	21.4
360	-152.6	146.1	-0.1	20.0

2.4.2 **Computed Gravimetric Geoid Undulations**

The geoid undulation contributions from the EGM96 and reference gravity anomalies Δg_{GM} are computed with (2.2) and (2.8) respectively using 45, 60, 90, 120, 180, 240, and 360 spherical harmonic expansions. For each degree of expansion, the block size used in the Stokes integration varies between 1°×1° and 15°×15°, which correspond respectively to the smallest and largest cap sizes used in this analysis. The results of $N_{\Delta g_r}$ are then added to the corresponding geoid contribution from the EGM96, as well as the geoid topographic indirect effect, which is computed with all the data points in each block.

2.4.2.1 Absolute Geoid Error with respect to GPS/leveling

The statistics of the standard deviation (Std) of the absolute differences between the two types of geoid undulations at 265 GPS benchmark stations are summarized in Table 2.2. The systematic datum differences between the gravimetric geoid and the GPS/levelling geoid (Kotsakis and Sideris, 1999) are removed by a four-parameter transformation equation. See Heiskanen and Moritz (1967) for details. The Std of the absolute difference after a least-squares fit with a four-parameter model is also given (in parentheses) in Table 2.2. Figures 2.1 and 2.2 show the graphs of absolute geoid difference Std values against the degree of expansion and cap size, respectively.

Table 2.2: Comparison of gravimetric geoid with GPS/levelling derived geoid before and after (in parenthesis) datum fit

Cap Size	**Degree of Spherical Harmonic Expansion**					
	60 (m)	90 (m)	120 (m)	180 (m)	240 (m)	360 (m)
Zero	1.04 (0.94)	0.72 (0.66)	0.64 (0.59)	0.52 (0.46)	0.45 (0.39)	0.43 (0.35)
1	0.49 (0.40)	0.34 (0.31)	0.30 (0.27)	0.25 (0.20)	0.24 (0.20)	0.24 (0.20)
3	0.38 (0.31)	0.29 (0.24)	0.24 (0.19)	0.24 (0.20)	0.24 (0.19)	0.25 (0.19)
5	0.35 (0.25)	0.28 (0.22)	0.23 (0.18)	0.23 (0.20)	0.22 (0.19)	0.22 (0.19)
7.5	0.32 (0.17)	0.27 (0.18)	0.22 (0.16)	0.18 (0.15)	0.18 (0.15)	0.18 (0.15)
10	0.22 (0.14)	0.20 (0.14)	0.18 (0.13)	0.15 (0.13)	0.15 (0.13)	0.15 (0.13)
12.5	0.22 (0.16)	0.19 (0.15)	0.18 (0.14)	0.15 (0.13)	0.15 (0.14)	0.15 (0.14)
15	0.21 (0.16)	0.19 (0.15)	0.18 (0.14)	0.15 (0.13)	0.15 (0.14)	0.15 (0.14)

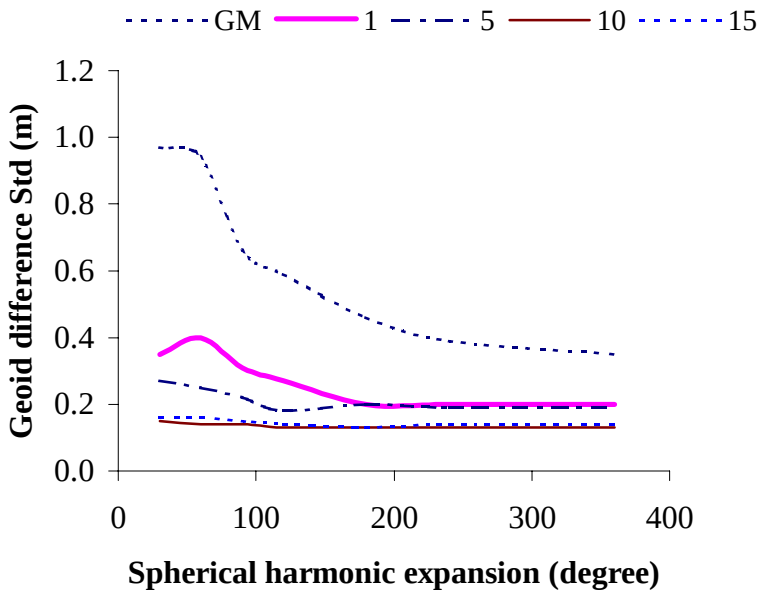

Figure 2.1: Absolute geoid accuracy versus harmonic degree of expansion

Legend values are block sizes in degrees

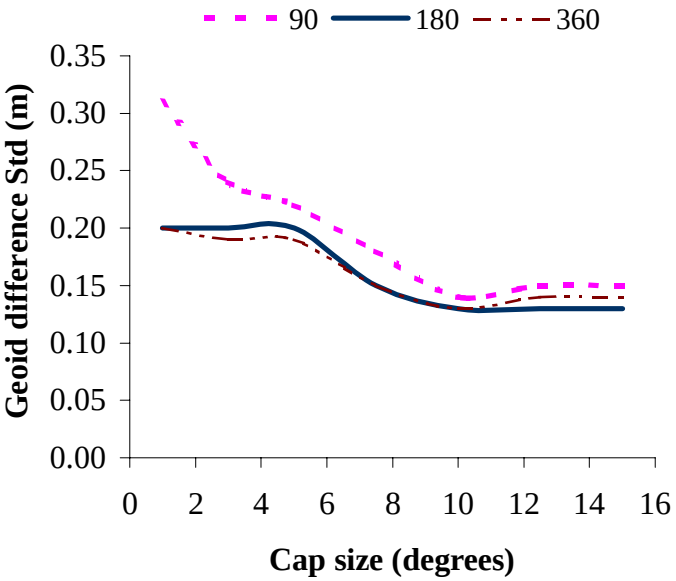

Figure 2.2: Absolute geoid accuracy versus Stokes's cap size

Legend values are spherical harmonic degree

As shown in Table 2.2, the gravimetric geoid computed with larger cap size, which corresponds to more local gravity data, gives better results. Figure 2.1 shows that the improvement in the accuracy of the geoid estimated with harmonic expansion greater than 200 degrees and cap size of 10° ×10° or greater is negligible. Figure 2.2 shows that the improvement in the accuracy of the computed geoid when the block size is increased beyond 10°×10° is of the order of few mm.

Combining the results of Figure 2.1 and 2.2, it is evident that the best estimates of the geoid can be obtained with spherical harmonic expansion of about 200 degree and Stokes's integration with local gravity data in a capsize of 10° × 10°. Results computed with degree of expansion greater than 200 degree and cap size greater than 10° × 10° do not seem to improve the accuracy of the geoid estimates.

2.4.2.2 Relative Geoid Error with respect to GPS/leveling

To evaluate the relative agreement of the computed gravimetric geoid with respect to the GPS/leveling data, relative differences are formed on baselines of 100km and 500km in length. The relative accuracy values are the average value over the baselines with length about ± 10km from the nominal value. The results of the Std of relative geoid differences are plotted against the degree of spherical harmonic expansion in Figures 2.3 and 2.5 for the 100km and 500km baselines respectively. Figures 2.4 and 2.6 show the graph of the relative geoid Std against cap size, for 100km and 500km baselines respectively. Again the results of Figures 2.3 to 2.6 agree with the previous results shown in Figures 2.1 and 2.2 for the Std of absolute geoid differences. In order to obtain geoid with a relative accuracy of 1.5ppm on 100km baseline, EGM96 solution with a minimum of 200 spherical harmonic expansion, as well as Stokes's integration with local data in cap size of 5°×5° or more is required. In Figures 2.3 and 2.5, the legend values are the cap sizes in degrees; while in Figures 2.4 and 2.6, the legend values are spherical harmonic degree.

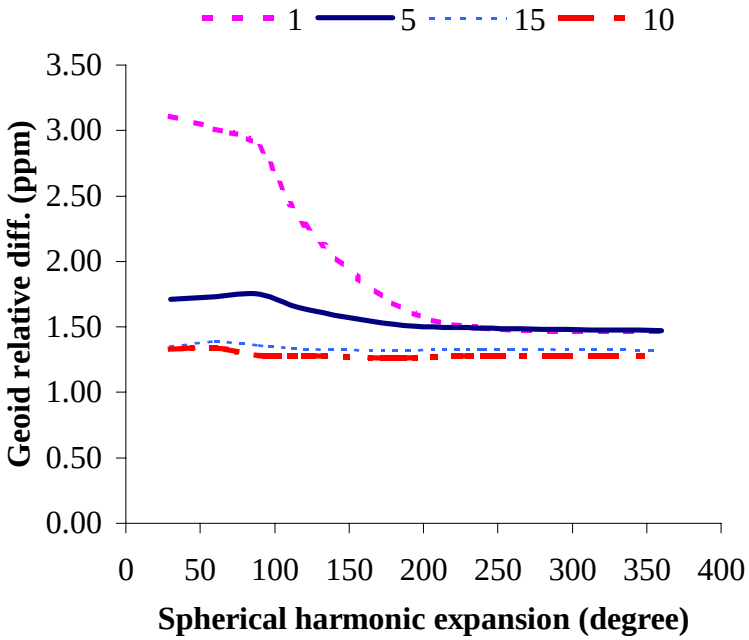

Figure 2.3: Relative geoid accuracy versus degree of expansion for 100 km baselines

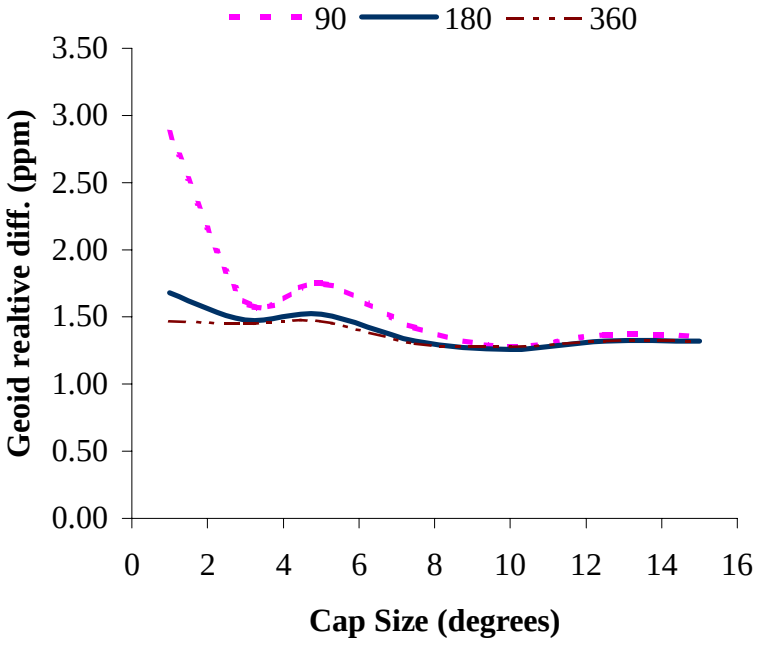

Figure 2.4: Relative geoid accuracy versus Stokes's cap size for 100 km baselines

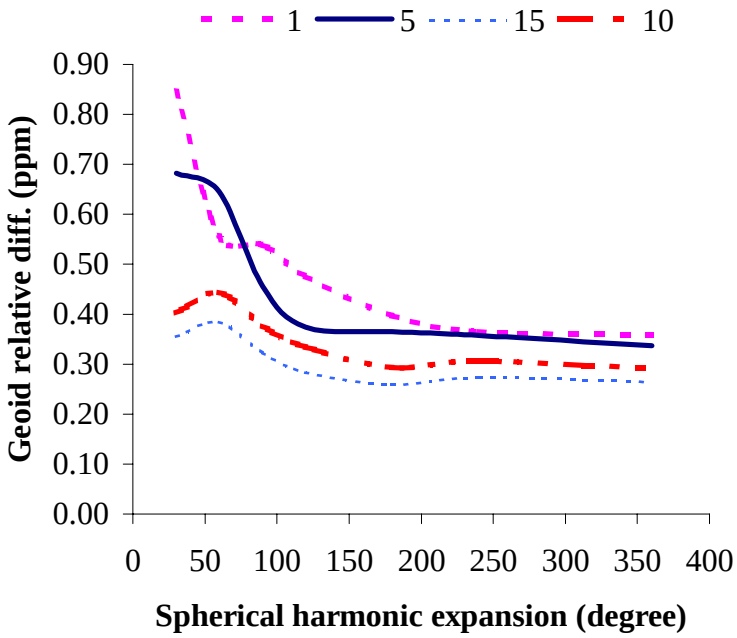

Figure 2.5: Relative geoid accuracy versus degree of expansion for 500 km baselines

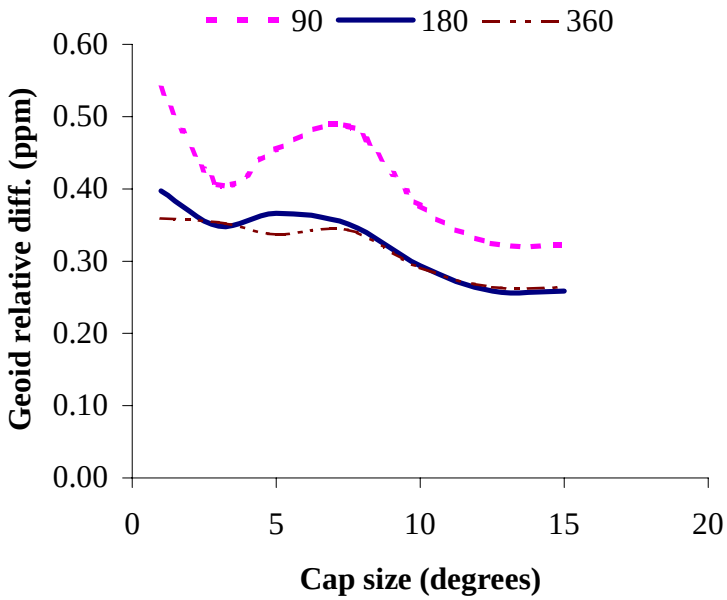

Figure 2.6: Relative geoid accuracy versus Stokes's cap size for 500 km baselines

2.5 THE EFFECT OF LATERAL DENSITY VARIATIONS ON TERRAIN CORRECTIONS AND GEOID UNDULATIONS

The terrain correction formula based on the mass prism or mass line model (Li, 1993) is usually executed with constant topographic density value ($\rho_o = 2.67\,\mathrm{gm/cm^3}$) for most applications. In this section, rigorous terrain correction formulas in which the earth topographic mass is represented by mass prisms of equal base area is used to estimate terrain corrections with actual topographic density values, as well as with a constant topographic density value. The effect of making the assumption of constant density values for the terrain correction, as well as for estimating geoid undulation, is investigated for five areas located in the Rocky Mountains of western Canada.

Table 2.3: Statistics of topographic densities and heights

Test Area	**SW corner coordinate**		**Density** (g/cm**3)			**Height** (m)		
	Lat.	Long.	Min	Max	Std	Min	Max	Std
DRKY1	49	-116	2.49	2.85	2.57	700.00	3377.00	1697.78
DRKY2	49	-120	2.49	2.90	2.68	170.00	2814.00	1281.64
DRKY3	51	-120	2.56	2.90	2.60	386.00	3506.00	1639.44
DRKY4	49	-122	2.49	2.98	2.70	0.00	2754.00	1284.57
DRKY5	51	-122	2.56	2.90	2.71	294.00	2803.00	1265.98

The terrain corrections for selected areas are computed using equations (2.13) and (2.14) with actual topographic density values, and with constant topographic density value of $2.67\mathrm{g/cm^3}$. Table 2.3 shows the statistics of the topographic density data and heights, as

well as the location of the test areas. The results of the terrain corrections, and their differences are presented in Table 2.4.

Figures 2.6 and 2.7 show contour plots of the topographic heights and the differences between the two estimated terrain corrections. Each figure contains the plot for the areas DRKY3 and DRKY5 at the top and bottom, respectively.

Table 2.4: Statistics of terrain corrections with and without topographic density variations

Test Area	**Without density variations** (mGal)			**With density variations** (mGal)			**Difference** (mGal)		
	Min	Max	Std	Min	Max	Std	Min	Max	Std
DRKY1	0.10	50.39	6.65	0.10	50.37	6.44	-0.58	2.27	0.24
DRKY2	0.33	50.04	6.23	0.33	46.78	6.24	-1.28	3.26	0.20
DRKY3	0.82	75.27	11.35	0.82	77.99	11.64	-2.73	3.82	0.45
DRKY4	0.23	60.52	7.69	0.23	60.12	7.71	-1.95	3.18	0.22
DRKY5	0.05	46.45	5.13	0.05	48.40	5.29	-1.95	1.38	0.21

Geoid undulations are estimated with equation (2.12) using reduced gravity anomalies that are derived with the two different terrain corrections. The result of the difference between the geoid undulations estimated with actual topographic density and constant topographic density is shown in Figure 2.9 for DRKY3 and DRKY5 at the top and bottom, respectively. The Statistics of the difference is also given in Table 2.5.

Table 2.5: Statistics of geoid undulations with and without topographic density variations

Test Area	**Without density variation** (cm)			**With density variation** (cm)			**Difference** (cm)		
	Min	Max	Std	Min	Max	Std	Min	Max	Std
DRKY1	-165.7	118.7	69	-1.673	1.173	70	0.7	2.1	1.6
DRKY2	-170.1	110.6	88	-1.704	1.103	88	-0.7	0.8	0.3
DRKY3	-10.6	256.0	139	-0.116	2.53	137	-0.1	3.8	2.5
DRKY4	-125.0	177.5	72	-1.248	1.776	72	-1.2	0.8	0.4
DRKY5	-154.3	122.2	76	-1.544	1.205	76	-0.5	1.8	0.8

Geoid indirect effect is estimated using equation (2.10) with and without topographic density variations. The result of the differences between the two geoid indirect effects is shown in Figure 2.10 for DRKY3 and DRKY5 at the top and bottom, respectively. The two components of the geoid from the terrain correction and topographic indirect effect on the geoid are then combined under the assumption of perfect (linear) correlation between the two components. The result of the geoid difference from the total effect of the two components is shown in Figure 2.11, for DRKY3 and DRKY5 at the top and bottom, respectively. The Statistics of the geoid indirect effects differences are given in Table 2.6 while those of the combined geoid effects differences are given in Table 2.7.

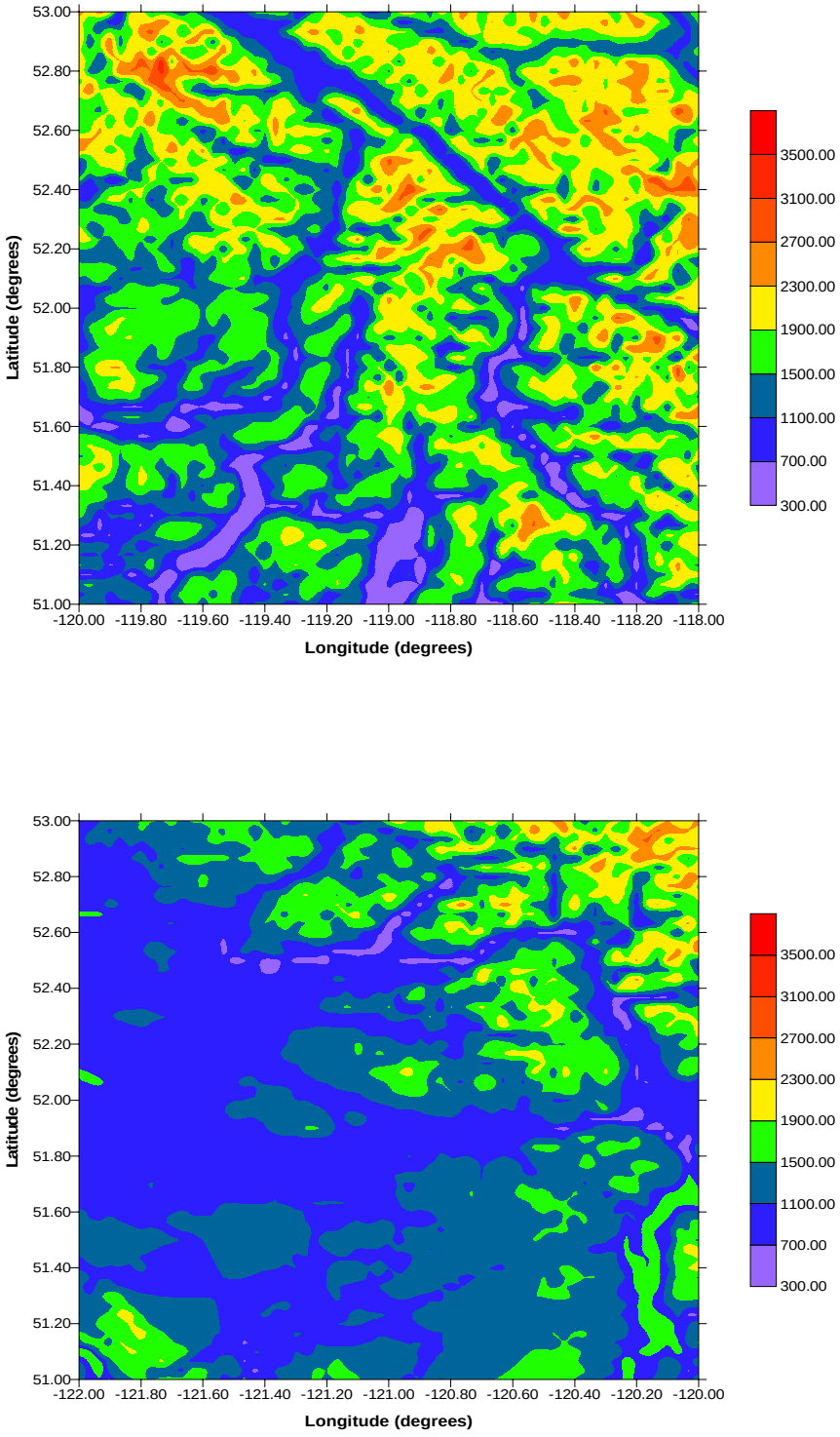

Figure 2.7: Contour plots of topographic heights for DRKY3 and DRKY5, in metres

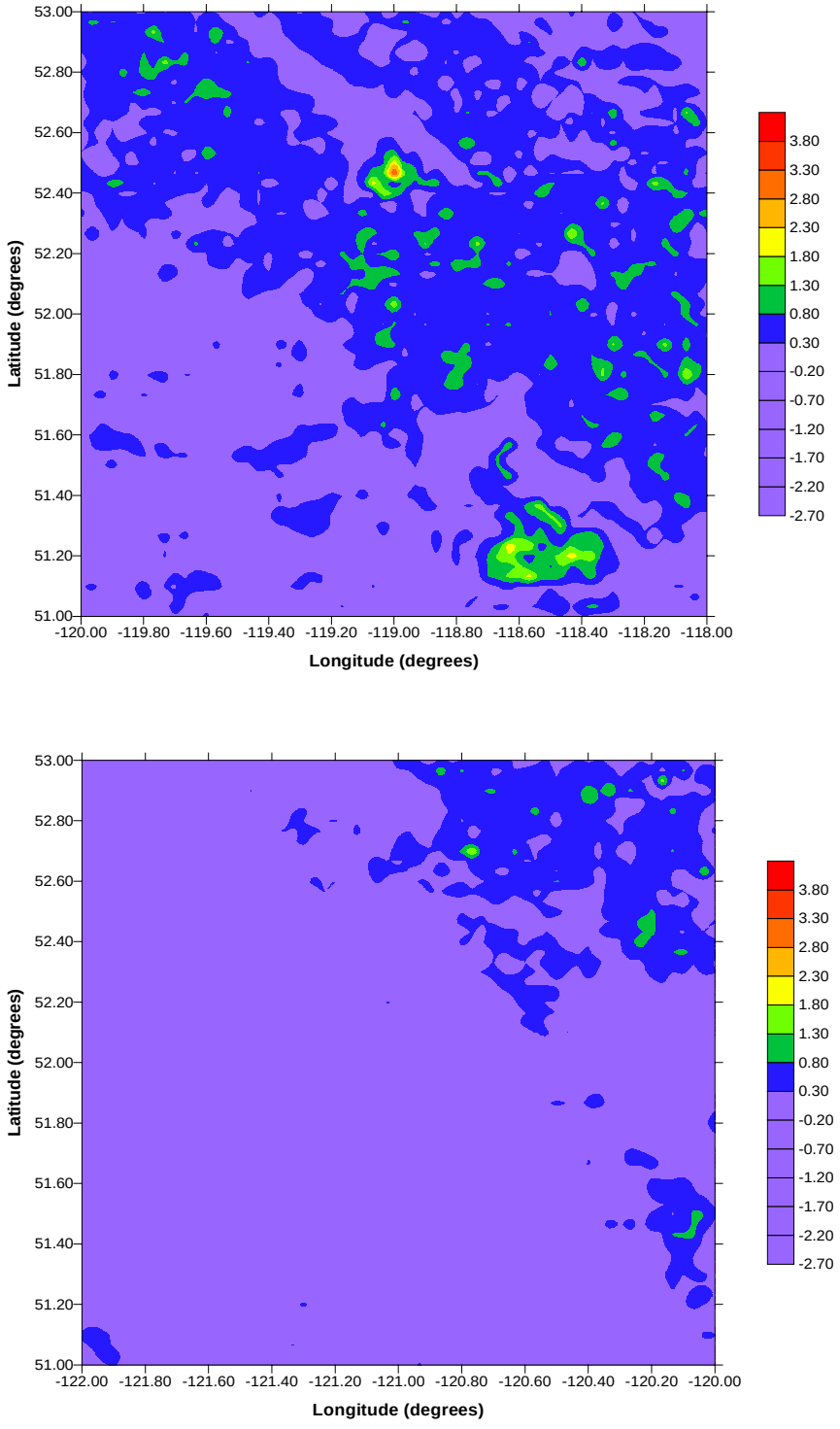

Figure 2.8: Contour plots of terrain correction differences for DRKY3 and DRKY5, in mGal

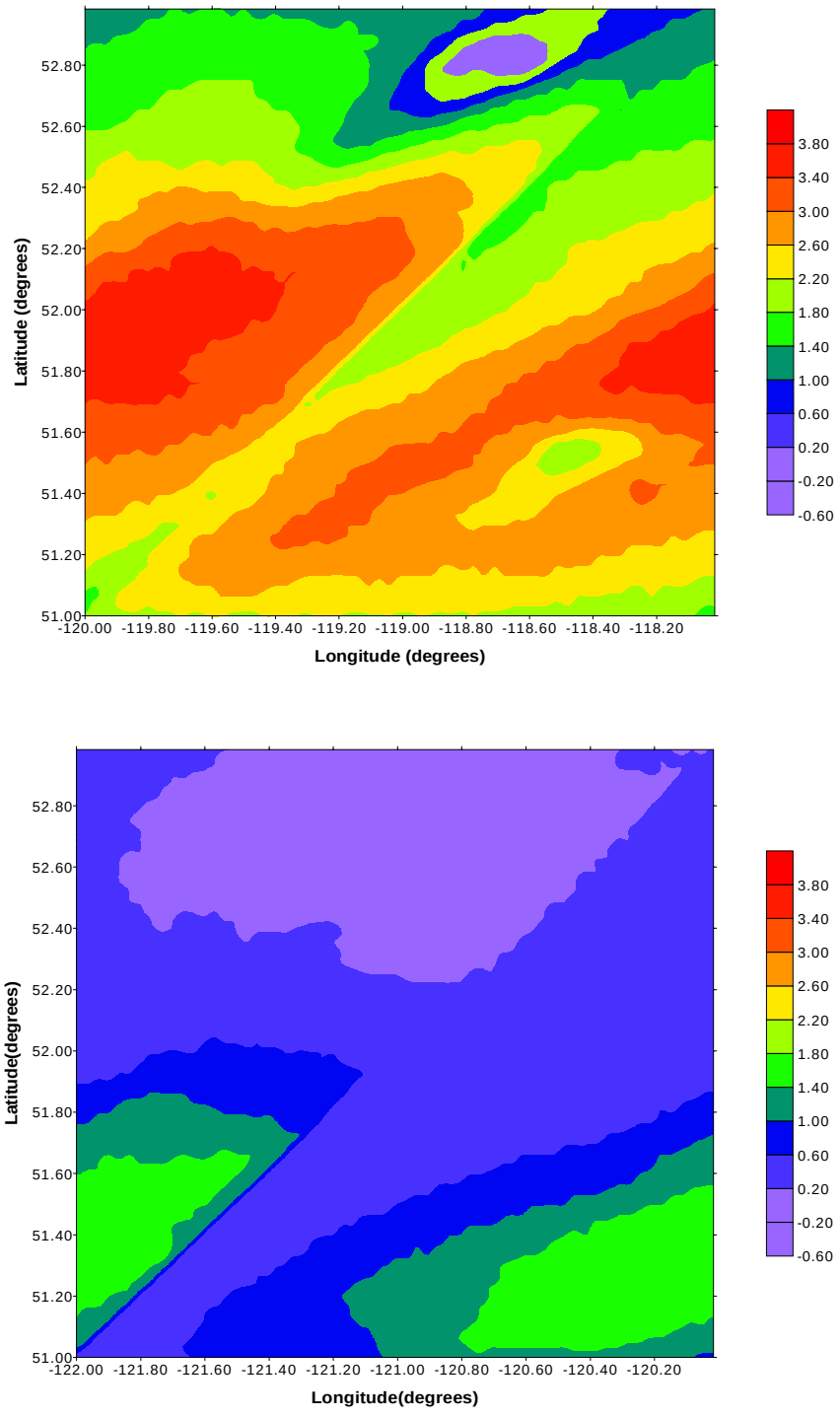

Figure 2.9: Contour plots of geoid undulation differences for DRKY3 and DRKY5, in cm

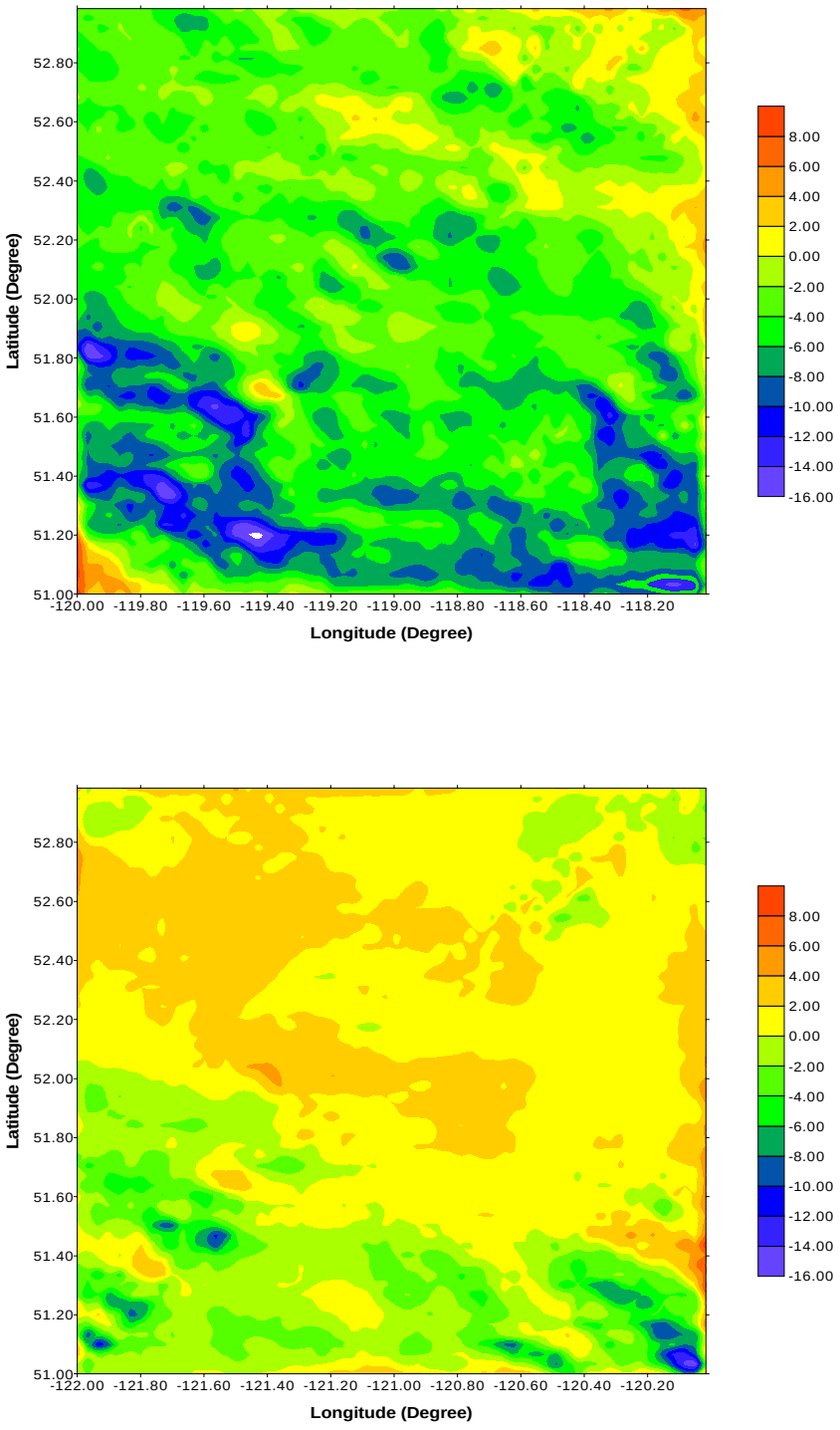

Figure 2.10: Contour plots of geoid indirect effect differences for DRKY3 and DRKY5 in cm

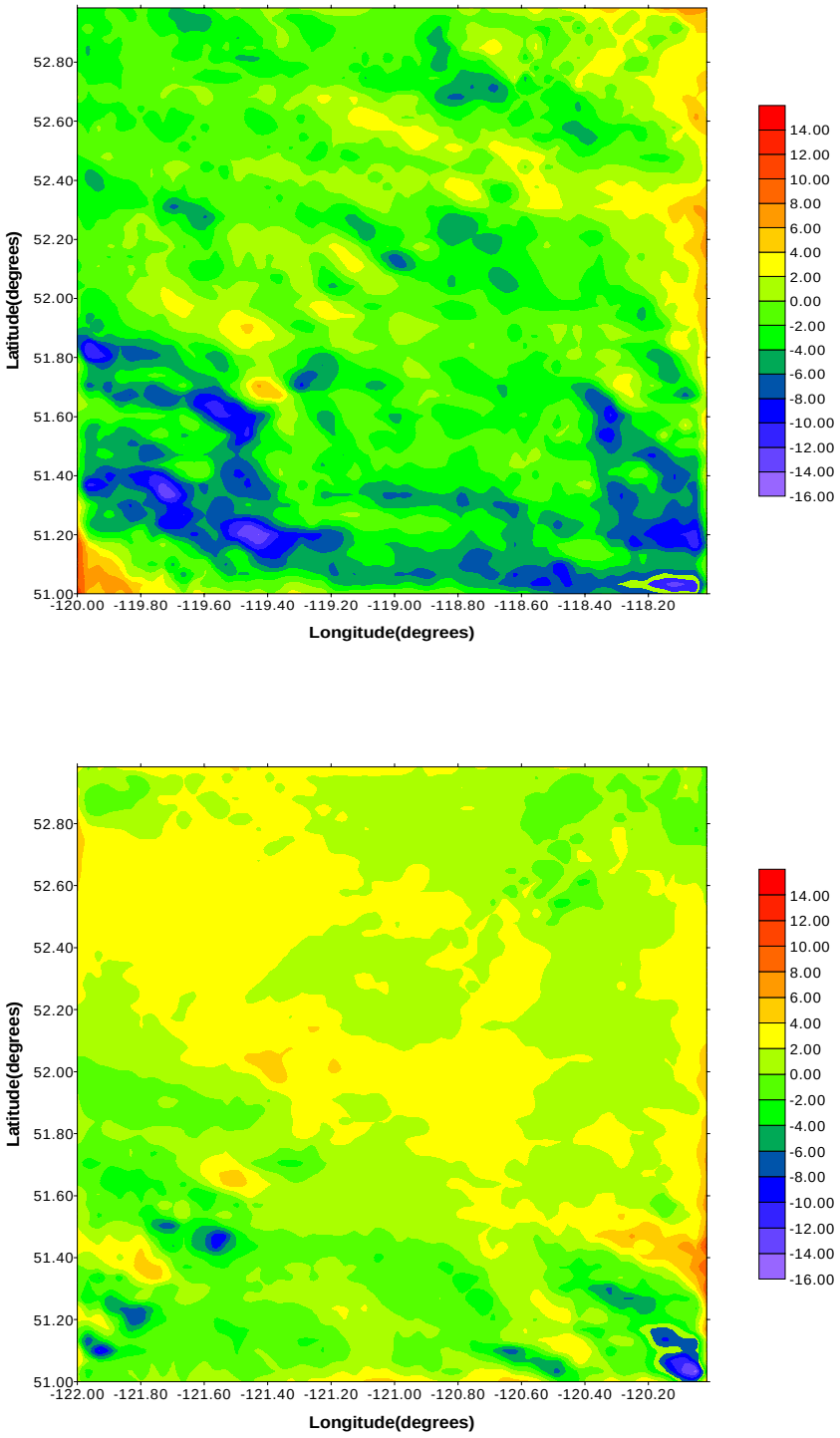

Figure 2.11: Contour plots of geoid direct and indirect effect differences for DRKY3 and DRKY5 in cm

Table 2.6: Statistics of geoid indirect effect with and without topographic density variations

Test Area	**Without density variation** (cm)			**With density variation** (cm)			**Difference** (cm)		
	Min	Max	Std	Min	Max	Std	Min	Max	Std
DRKY1	-39.9	-2.9	7.1	-30.3	2.5	6.5	-14.6	12.3	2.5
DRKY2	-28.1	-0.7	5.2	-28.4	2.5	5.1	-6.3	16.9	1.4
DRKY3	-39.8	-1.4	6.8	-30.2	7.0	5.8	-17.3	12.2	3.2
DRKY4	-27.1	5.5	4.8	-27.1	5.5	4.8	-6.8	19.7	1.5
DRKY5	-31.1	-1.4	4.6	-24.5	4.0	3.7	-15.3	9.2	2.2

Table 2.7: Statistics of geoid direct and indirect effect with and without topographic density variations

Test Area	**Without density variation** (cm)			**With density variation** (cm)			**Difference** (cm)		
	Min	Max	Std	Min	Max	Std	Min	Max	Std
DRKY1	-180.9	100.3	54.3	-178.4	102.3	54.1	-12.7	13.2	2.4
DRKY2	-177.5	89.6	50.0	-179.5	92.4	50.2	-5.6	17.0	1.4
DRKY3	-22.0	241.6	61.8	-27.8	241.9	62.3	-14.9	14.0	3.0
DRKY4	-128.9	161.4	68.6	-131.7	161.9	68.8	-7.1	19.5	1.5
DRKY5	-156.2	111.1	63.6	-157.8	112.7	64.6	-14.2	10.8	1.9

It is evident in Figures 2.6 and 2.7 that the terrain correction difference is correlated with the topography of the local area. In addition, the results in Table 2.5 and Figure 2.9 show that a geoid difference of up to 4cm could be omitted in areas with very high topography if constant density value is used instead of actual values for terrain correction estimation.

The effect of using actual density values is more noticeable in the computation of the geoid indirect effect. The results in Table 2.6 and Figure 2.10 show that a difference of up to 20 cm could be omitted in the geoid estimates. When the two geoid components are combined, a geoid difference of 20 cm is noticed (Table 2.7 and Figure 2.11).

CHAPTER 3

ESTIMATION AND MODELLING OF GRAVITY FIELD COVARIANCE AND POWER SPECTRAL DENSITY FUNCTIONS

This chapter outlines the basic concepts of covariance, correlation and power spectral density (PSD) function estimation and the relation between the three functions. Formulas that are used in the spectral analysis are also presented.

Section 3.1 discusses the basic concepts of covariance, correlation and power spectral density functions; it also highlights the relationship between the three functions. In section 3.2, formulas used for practical estimation of empirical gravity anomaly covariance function, as well as covariance function models, are presented. Section 3.3 discusses the computation of gravity anomaly PSD function, and the relationship between the PSD function and degree variances is presented in section 3.4.

3.1 CONCEPTS OF COVARIANCE AND SPECTRAL DENSITY FUNCTIONS

This section discusses the basic concepts of covariance, correlation and power spectral density functions and the relation between the three functions. The derivations of the equations relating the functions is not discussed as it can be found in many text books and papers on the subject; see, e.g., Bendat and Piersol (1980, 1986) and Sideris (1994). The definition of these functions is limited in this section to Cartesian coordinates with the X axis pointing east, the Y axis pointing north and the Z axis pointing upward.

The covariance function $C_{gh}(x,y)$ of two functions $g(x_1,y_1)$ and $h(x_2,y_2)$, which are sample functions of the corresponding stationary random processes, is defined as

$$C_{gh}(\Delta x,\Delta y) = E\left[\left(g(x_1,y_1)-\bar{g}\right)\left(h(x_2,y_2)-\bar{h}\right)\right] \tag{3.1}$$

where $\Delta x = x_2 - x_1$, $\Delta y = y_2 - y_1$, $E[\ ]$ is the mathematical expectation operator, and $\bar{g}$ and $\bar{h}$ are the mean values of the functions $g(x_1,y_1)$ and $h(x_1,y_1)$, respectively. When the two functions $g(x_1,y_1)$ and $h(x_2,y_2)$ are identical, i.e., $h(x_1,y_1) = g(x_2,y_2)$, then the result of equation (3.1) is termed auto-covariance function. Otherwise, if $h(x_1,y_1) \neq g(x_2,y_2)$, the resultant covariance is known as the cross-covariance function. Furthermore, if $C_{gh}(\Delta x,\Delta y)$ is such that it could be replaced with $C_{gh}(s)$, where $s^2 = \Delta x^2 + \Delta y^2$, then the resultant covariance function is said to be isotropic.

The correlation function $R_{gh}(x,y)$ of two sample functions $g(x_1,y_1)$ and $h(x_2,y_2)$ is defined as

$$R_{gh}(\Delta x,\Delta y) = E\left[\left(g(x_1,y_1)\right)\left(h(x_2,y_2)\right)\right] \tag{3.2}$$

where all variables have the same meaning as previously defined. For sample functions with zero means, i.e., $\bar{g} = \bar{h} = 0$, the correlation function is identical to the covariance function, i.e., $R_{gh} = C_{gh}$. Sample functions with zero means are referred to as centred functions. Again, if the two sample functions are identical, the correlation function in equation (3.2) is known as the auto-correlation function. Otherwise, it is called cross-correlation function.

The PSD function is defined as the frequency domain equivalent of the correlation function. The function contains the spectrum of the mean square values of the sample functions. For the two sample functions $g(x_1, y_1)$ and $h(x_2, y_2)$, the PSD function $P_{gh}(x, y)$ is defined via the Fourier transform of the correlation function $R_{gh}(x, y)$ as

$$P_{gh}(u, v) = \int_{-\infty}^{\infty} \int_{-\infty}^{\infty} R_{gh}(x, y) e^{-j2\pi(ux+vy)} dxdy = \mathbf{F}\{R_{gh}(x, y)\} \tag{3.3}$$

where the spatial frequencies u and v (also known as wave numbers) correspond to x and y, respectively. If the two functions $g(x_1, y_1)$ and $h(x_2, y_2)$ are centered functions, then equation (3.3) is equivalent to

$$P_{gh}(u, v) = \int_{-\infty}^{\infty} \int_{-\infty}^{\infty} C_{gh}(x, y) e^{-j2\pi(ux+vy)} dxdy = \mathbf{F}\{C_{gh}(x, y)\} \tag{3.4}$$

since in this case the covariance and correlation functions are equal. Again we have auto-power spectral density function if the two sample functions are identical and cross-power spectral density function if otherwise.

In practice, discrete values of the sample functions are usually given on a finite plane. Therefore, the continuous spectrum given in equation (3.3) and (3.4) becomes discrete. The discrete Fourier transform is then applied. In addition, the expressions in (3.1) and (3.2) are executed as summation in the x and y directions. The derivation of the expressions for the covariance, correlation and PSD functions, and their general applications can be found in Bendat and Piersol (1980, 1986).

3.2 LOCAL GRAVITY ANOMALY COVARIANCE FUNCTION

Moritz (1980) gave the basic definition of a global covariance function on a sphere as the expected value over the sphere of the product of all pairs of gravity values located at fixed distances apart. The local covariance function of the gravity field is defined by Goad et al, (1984) as a special case of a global covariance function where the information content of wavelengths longer than the extent of the local area has been removed, and the information outside, but nearby, the area is assumed to vary in a manner similar to the information within the area. In this section, the fundamental equations for the estimation of local covariance functions for gravity anomalies are presented. The notation employed in the expressions for the covariance functions follow closely the one used in Heiskanen and Moritz (1967).

Three parameters are used to describe the characteristics of the local covariance function of gravity field quantities. The definition of the three parameters, the variance C_0, the correlation distance $\chi_{1/2}$ and the horizontal gravity gradient variance, are given in Moritz (1980).

The first two parameters C_0 and $\chi_{1/2}$ (Figure 3.1) are used in this study to describe the local covariance function of the gravity anomalies. The variance C_0 is the value of the covariance for zero distance while the correlation distance $\chi_{1/2}$ is defined as the distance at which the covariance is half of the variance value, i.e. $C(\div_{1/2}) = \frac{1}{2} C_0$.

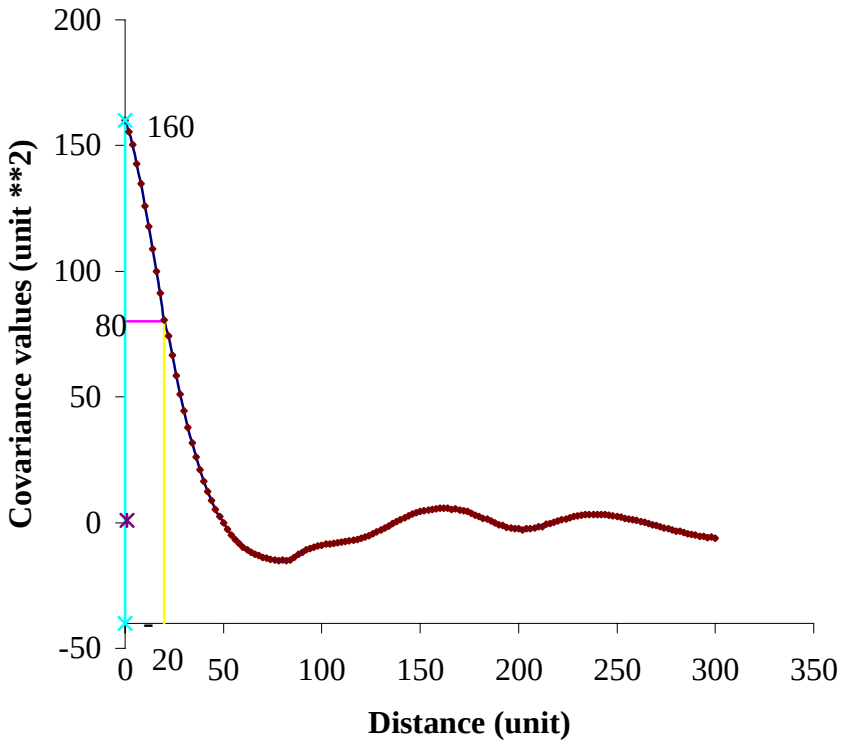

Figure 3.1: Local covariance function parameters, $C_0 = 160$, $\chi_{1/2} = 20$

In the sequel, two observations g and h at (φ, λ) and (φ′, λ′) respectively on the spherical earth surface are assumed to be linear functionals of the anomalous potential T, with information content of the wavelength longer than the extent of the local area removed. The covariance function between g(φ, λ) and h(φ′, λ′) is given as

$$C_{gh}(\psi) = \frac{1}{A}\int_{\varphi_1}^{\varphi_2}\int_{\ddot{e}_1}^{\ddot{e}_2}\int_{0}^{2\eth}\frac{1}{2\eth}\, g\, h\cos(\psi)\, d\acute{a}\, d\varphi\, d\ddot{e} \qquad (3.5)$$

where A is the size of the area on the unit sphere, $\varphi_1, \varphi_2, \ddot{e}_1, \ddot{e}_2$ represents the extent of the local area, á is the azimuth and $\cos(\psi) = \sin\varphi\sin\varphi' + \cos\varphi\cos\varphi'\cos(\ddot{e} - \ddot{e}')$.

Equation (3.5) represents a homogenous and isotropic covariance function, which is calculated as an average of the product of g and h over the local area (homogeneity) and as an average over the azimuth (isotropy). In practice, the observations are at discrete points in the local area and the integral reduces to numerical summation.

3.2.1 **Estimation of Empirical Covariance Function**

Two methods are usually employed in the estimation of the local gravity empirical covariance function. The first method makes use of the actual data available to compute the empirical covariance functions directly, while the second method computes the empirical covariance functions by taking the inverse Fourier transform of PSD functions. The former method is referred to as the direct method while the later is referred to as the indirect method.

3.2.1.1 Covariance Function from Actual Data

This method computes the empirical covariance function directly from actual data and is referred to as the direct method. Two formulas are presented for empirical covariance estimation with actual gravity data. The first set of formulas estimate the isotropic empirical covariance function of gravity data with irregular distribution. For gravity data with a regular grid, the empirical covariance function is given by the second set of formulas.

The covariance function between the function g and h given at discrete points in blocks on the sphere is given as

$$C(\psi) = \frac{\sum a_g \, a_h \, g(\varphi, \ddot{e}) \, h(\varphi', \ddot{e}')}{\sum a_g a_h} \tag{3.6}$$

where a_g and a_h represent the area of the blocks on the sphere for observation g and h, respectively. For gravity anomalies, $g(\varphi, \ddot{e}) = \Delta g_i$ and $g(\varphi', \ddot{e}') = \Delta g_j$, equation (3.6) provides an isotropic gravity anomaly covariance function.

If the gravity anomalies for example are given in blocks of equal area, then equation (3.6) reduces to

$$C_{\Delta g \Delta g}(\psi_k) = \frac{\sum_k \Delta g_i \Delta g_j}{n_k} \tag{3.7}$$

where n_k represents the number of products taken at a given spherical distance ψ_k. The distance ψ to which product at ψ_k is determined is defined by

$$\psi - \frac{\ddot{A}\,\psi}{2} < \psi_k < \psi + \frac{\ddot{A}\,\psi}{2} \tag{3.8}$$

where $\Delta\psi$ is a suitable interval.

In the case of gravity anomalies given on a rectangular regular grid of area size $T_x \times T_y$ and with grid spacing Δx and Δy in the x and y directions, respectively, the empirical non-isotropic covariance function for gravity anomalies Δg is estimated as

$$C_{\Delta g \Delta g}(k,l) = \frac{1}{M-k}\frac{1}{N-l}\sum_{i=0}^{M-k-1}\sum_{j=0}^{N-1-l}\Delta g(i,j)][\Delta g(i+k, j+l)] \qquad (3.9)$$

where $M = \frac{T_x}{\Delta x}$, $N = \frac{T_y}{\Delta y}$.

3.2.1.2 Covariance Function via Spectral Density Function

The empirical covariance function could be estimated indirectly from gridded data by the fast Fourier transform (FFT) algorithm. Since the power spectral density function is the frequency domain equivalence of the correlation function, then for centered gravity data, the inverse Fourier transform of the PSD function provides the corresponding covariance function of the gravity data.

In flat earth approximation, the surface of the earth is replaced by a tangential plane. The spherical distance (ψ) becomes the planar distance s $(s^2 = x^2 + y^2)$. In a local area, both approximations converge to each other (Knudsen, 1987). The PSD function (actually the periodogram) of gravity anomaly observations is estimated by Fourier transform as

$$P_{\Delta g \Delta g}(u,v) = \Delta G(u,v)\Delta G(u,v)^{*} \tag{3.10}$$

where ΔG is the Fourier transform of the gravity anomaly observations Δg.

The two-dimensional non-isotropic covariance function $C_{\Delta g \Delta g}(x,y)$ is then estimated by taken the inverse Fourier transform of $P_{\Delta g \Delta g}(u,v)$ as

$$C_{\Delta g \Delta g}(u,v) = \mathbf{F}^{-1}\{P_{\Delta g \Delta g}\} = \int_{-\infty}^{\infty}\int_{-\infty}^{\infty} P_{\Delta g \Delta g}(u,v) e^{j2\pi(ux+vy)} dxdy \tag{3.11}$$

An isotropic covariance function $C_{\Delta g \Delta g}(s)$ is derived from equation (3.11) by averaging over all azimuths as

$$C_{\Delta g \Delta g}(s) = \frac{1}{2\pi}\int_{0}^{2\pi} C_{\Delta g \Delta g}(x,y) d\acute{a} \tag{3.12}$$

For isotropic PSD function $P_{\Delta g \Delta g}(\grave{u})$, where $\grave{u}^2 = u^2 + v^2$, the corresponding isotropic covariance function $C_{\Delta g \Delta g}(s)$, is obtained by the inverse Hankel transform and not with the inverse Fourier transform; see Forsberg 1984 for details. The Hankel transform operator $\mathbf{H}$ and its inverse $\mathbf{H}^{-1}$ is define for the function g as

$$g(\grave{u}) = \mathbf{H}\{g(s)\} = \int_{0}^{\infty} s g(s) J_0(s\grave{u}) ds \tag{3.13}$$

$$g(s) = \mathbf{H}^{-1}\{g(\psi)\} = \int_0^{\infty} \psi g(\psi) J_0(s\psi) d\psi \qquad (3.14)$$

where J_0 is the Bessel function of order zero.

3.2.2 **Modeling of the Gravity Anomaly Covariance Function**

In gravity field prediction with heterogeneous gravity field data, self sufficient covariance models are required in the estimation method. The self-sufficiency of the covariance functions ensures that the covariance functions of the different gravity field quantities are related through linear functional of the anomalous potential. A self sufficient covariance function is derived by fitting empirical covariance values to some analytical function, which is usually characterized by few parameters.

Various covariance models for gravity field signals are presented in Moritz (1980). A number of analytical covariance functions have also been suggested and used for gravity field approximation in flat earth approximation. See Vassiliou and Schwarz (1987) and Jordan (1972) for details.

For spherical earth, the covariance function model is usually derived from degree a variance model. The Tscherning/Rapp model (Tscherning and Rapp, 1974) is the most widely used degree variance models, and is adopted in this study for covariance modelling. Empirical covariance values are fitted to the analytical model by least squares in an iterative procedure.

The covariance function $K(\psi)$ of the anomalous potential T expanded into a harmonics series is given in terms of Legendre polynomials as, (Moritz, 1980):

$$K(\psi) = \sum_{n=2}^{n_{max}} \sigma_n^2(T,T)\left(\frac{R_B}{r\,r'}\right)^{n+1} P_n(\cos\psi) \tag{3.15}$$

where n_{max} is the maximum degree and order of a global geopotential model that is used as the reference field, $\sigma_n^2(T,T)$ are the anomalous potential degree variances, r and r′ represent the geocentric radial distances of two observation points at a (spherical) distance ψ apart, and R_B is the radius of the Bjerhammar sphere.

Since in practice the covariance function $K(\psi)$ of the anomalous potential T cannot be estimated directly, equation (3.5) is fitted to covariance values of gravity field data that are linear functionals of T. The covariance of the local anomalous potential is then derived by applying the inverse linear functional relation. The covariance function of reduced local gravity anomalies derived from equation (3.15) can be expressed as

$$\begin{aligned} C_{\Delta g_r \Delta g_r}(\psi) = &\sum_{n=2}^{n_{max}} c_n^2(\Delta g_r, \Delta g_r) S^{n+2} P_n(\cos\psi) \\ &+ \sum_{n=n_{max}+1}^{\infty} \varepsilon_n^2(\Delta g_r, \Delta g_r) S^{n+2} P_n(\cos\psi) \end{aligned} \tag{3.16}$$

where $c_n^2(\Delta g_r, \Delta g_r)$ are the local gravity anomaly degree variances, $S = \left(\frac{R_B^2}{r\,r'}\right)$, Δg_r is the reduced gravity anomaly, and $\varepsilon_n^2(\Delta g_r, \Delta g_r)$ are the error degree variances of the local gravity data.

The degree variances of the potential and gravity anomalies are estimated using the Tscherning/Rapp model given as

$$\sigma_n^2(T,T) = \frac{A}{(n-1)(n-2)(n+24)} \tag{3.17}$$

$$\sigma_n^2(\Delta g,\Delta g) = \frac{(n-1)^2}{R_E^2}\sigma_n(T,T) \tag{3.18}$$

where A is a constant which is related to the variance value in unit of $mGal^2$. For other quantities of the gravity field, the covariance function and degree variances can be derived from the linear functional relation of such quantities to the anomalous potential. Expressions for other gravity field quantities can be found in Moritz (1980).

The error degree variances of the local gravity data $\varepsilon_n^2(\Delta g_r,\Delta g_r)$, is obtained by an approximate method with the following expressions:

$$\varepsilon_n^2(\Delta g_r,\Delta g_r) = \frac{1}{2\pi\tilde{a}}\frac{n+0.5}{(n-1)^2}P_{\varepsilon_{\Delta g}}(\grave{u}_n) \tag{3.19}$$

$$P_{\varepsilon_{\Delta g}}(\grave{u}_n) = \acute{o}_g{}^2 e^{\frac{\grave{u}_n}{a}},\ \grave{u}_n = \frac{n+0.5}{R} \tag{3.20}$$

where $P_{\varepsilon_{\Delta g}}$ is the isotropic gravity error PSD function, $\acute{o}_g$ is the average standard deviation of the gravity observations, and a is a constant (a=10). A detail expression for gravity error degree variances is given later in this thesis.

The fitting of the model in equation (3.16) to the empirical covariance values is done by an adjustment of the parameters R_B and A using a least square inversion method; see Knudsen (1987) for details. In the covariance analysis that follows, the modelling of the covariance functions is carried out with a computer program, which was originally written by Tscherning (1975). The program has been modified to suite the data format and error degree variance model in equation (3.19).

3.3 ESTIMATION OF THE GRAVITY ANOMALY POWER SPECTRAL DENSITY FUNCTION

The power spectral density (PSD) function can be estimated directly from the actual data in a grid by Fourier transform or indirectly by taken the inverse Fourier transform of previously estimated correlation function. For gravity anomalies given at discrete points on a plane, the PSD function can be computed directly from the data as

$$P_{\Delta g \Delta g}(u, v) = \mathbf{F}[\Delta g(x, y)]\mathbf{F}[\Delta g(x, y)]^{*} \qquad (3.21)$$

where * denotes complex conjugate, and $\mathbf{F}$ is the Fourier transform operator. Again, the evaluation of equation (3.21) by FFT requires that the gravity anomalies be on a grid. Further detail information on Fourier transform and its applications are found in Bracewell (1983) and Schwarz et al. (1990).

The second method used in the estimation of power spectral density function involves taking the Fourier transform of a previously calculated correlation function. For gravity anomalies Δg located at discrete points on a plane equation, (3.3) could be written as

$$P_{\Delta g \Delta g}(u, v) = \mathbf{F}\{R_{\Delta g \Delta g}(x, y)\} \tag{3.22}$$

where $\mathbf{F}$ denotes two-dimensional (2D) discrete Fourier transform operator. For centered gravity anomalies on a regular grid, the correlation function is equivalent to the covariance function given in (3.9).

3.4 RELATIONSHIP BETWEEN DEGREE VARIANCES AND POWER SPECTRUM

Degree variances are usually used to study the variation of the gravity field in various spectral bands because they allow easy comparison with results from global models. The degree variances of the anomalous potential σ_n^2 can be defined as the spectrum of the local isotropic covariance function of this potential in spherical earth approximation. Forsberg (1984) established a relationship between the degree variance σ_n^2 and the isotropic PSD function $P_{TT}(\omega)$ of the anomalous potential for flat earth approximations as

$$\sigma_n^2 = \frac{1}{2\pi R^2}\left(n + \frac{1}{2}\right) P_{TT}(\omega) \tag{3.23}$$

where the wave number $\omega = \dfrac{n + \frac{1}{2}}{R}$. In the sequel, two-dimensional PSD function of the gravity anomaly is computed first with equation (3.21) and made isotropic by averaging along circles of constant wavelength. Then the degree variances of the anomalous potential are estimated from

$$\sigma_n^2 = \frac{R^2}{(n-1)^2} c_n^2 \qquad (3.24)$$

where c_n is the degree variances of the local gravity anomalies estimated from the corresponding isotropic PSD function using an expression similar to (3.23) for the gravity anomaly.

CHAPTER 4

COVARIANCE ANALYSIS FOR AREAS IN CANADA

This chapter discusses the results of the empirical covariance functions for local gravity anomalies in selected areas across Canada. The preprocessing of the gravity anomaly data is discussed in section 4.1 while the results of both the space domain and frequency domain methods are presented and compared for all the selected areas in section 4.3. The selected mountainous areas are located in the west, the flat areas in the east and the marine areas in the Hudson bay, and the Pacific and Atlantic coasts of Canada. The mountainous areas have highly varying topography with standard deviation of 450m or higher. The flat areas are rather smooth with standard deviation usually below 200m.

4.1 TEST AREAS AND DATA REDUCTION

The results of the analysis in the sequel are based on data selected from blocks of $2^o \times 2^o$ in western (rocky areas) and eastern Canada (flat areas), and blocks of $5^o \times 5^o$ in marine areas. Figure 4.1 shows the location of all the test areas in rectangular blocks. In Table 4.1, the statistics of topographic heights, as well as the geographic local of the test areas are presented.

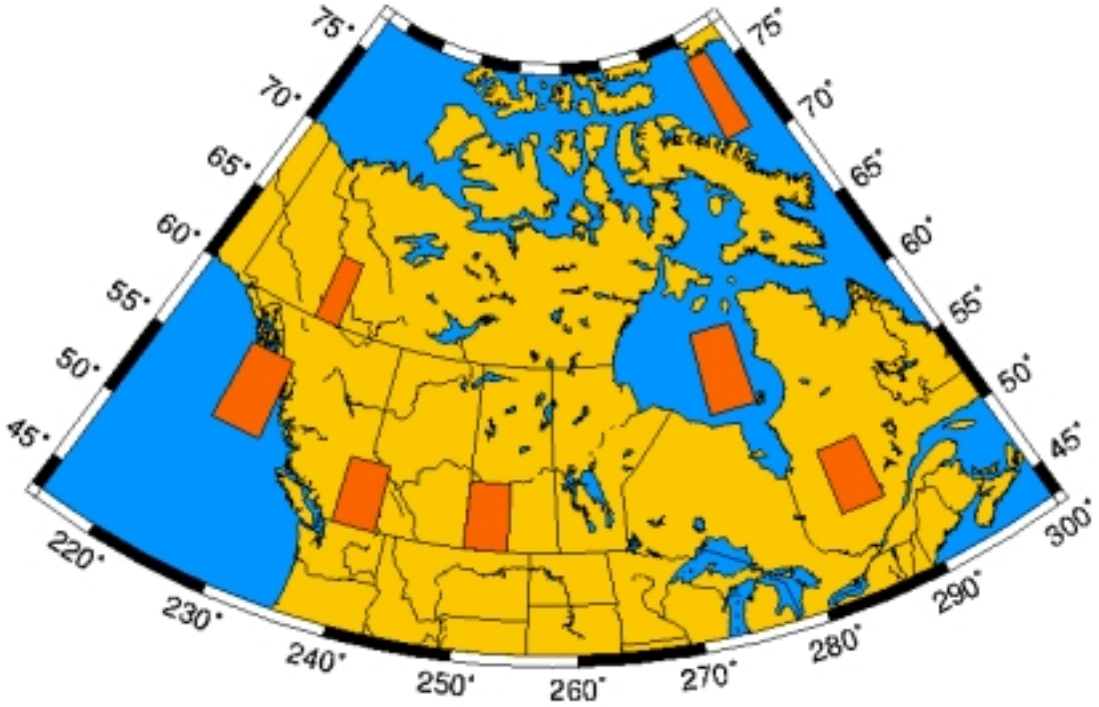

Figure 4.1: Distribution of test area blocks across Canada

Table 4.1: Covariance analysis test areas and height data statistics

Test Area	SW Corner Coordinate		Area Size (Block)	Height Statistics (m)			
	Lat.	Long.		Min	Max	Mean	Std
Mountainous Areas							
RK1	60	-131	$2^o \times 2^o$	627.09	2034.42	1167.24	376.43
RK2	62	-131	$2^o \times 2^o$	875.12	2275.23	1449.66	327.73
RK3	60	-129	$2^o \times 2^o$	600.39	2528.29	1234.63	436.33
RK4	62	-129	$2^o \times 2^o$	627.97	2449.13	1704.12	386.17
RK5	49	-120	$2^o \times 2^o$	282.55	2589.89	1047.07	601.17
RK6	51	-120	$2^o \times 2^o$	344.52	2910.97	1498.26	728.87
RK7	49	-122	$2^o \times 2^o$	6.10	2667.91	1122.01	517.26
RK8	51	-122	$2^o \times 2^o$	274.11	2822.00	1173.93	464.49
Flat Areas							
FT1	49	-110	$2^o \times 2^o$	563.88	1225.60	824.56	134.16
FT2	51	-110	$2^o \times 2^o$	500.79	771.14	668.16	49.94
FT3	49	-108	$2^o \times 2^o$	547.73	1000.35	746.32	94.31
FT4	51	-108	$2^o \times 2^o$	448.36	768.71	568.65	60.52
FT5	48	-76	$2^o \times 2^o$	280.11	502.92	391.24	41.47
FT6	50	-76	$2^o \times 2^o$	248.11	467.26	342.30	37.05
FT7	48	-74	$2^o \times 2^o$	99.67	572.41	307.15	146.05
FT8	50	-74	$2^o \times 2^o$	296.88	758.65	430.59	84.90
Marine Areas							
MR1	56	-85	$5^o \times 5^o$	0.00	49.38	0.01	0.50
MR2	52	-136	$5^o \times 5^o$	-2.60	2052.30	6.63	87.40
MR3	71	-70	$5^o \times 5^o$	0.00	0.00	0.00	0.00

For each selected area, the observed gravity anomalies are corrected for the terrain effect and the long wavelength part of the potential field was removed by subtracting the contribution from the EGM96 geopotential model, complete to degree and order 360. This corresponds to a wavelength of one degree, which is below the extent of the area blocks selected for analysis.

Table 4.2: Statistics of reduced gravity anomalies before and after gridding

(all values are in mGal)

Test Area	IPD (′)	Before Gridding				After centering (mean = 0) and gridding with 5′ and 1′ spacing					
						Min		Max		Std	
		Min	Max	Mean	Std	5′	1′	5′	1′	5′	1′
Mountainous Areas											
RK1	7.6	-68.5	67.6	-3.3	31.9	-70.3	-69.2	67.5	64.2	24.9	25.4
RK2	7.3	-72.6	87.9	10.0	31.1	-84.4	-74.7	73.3	68.4	20.1	20.4
RK3	6.9	-100.5	89.0	-3.3	43.8	-100.1	-91.1	81.2	78.0	31.6	32.1
RK4	7.8	-112.0	129.1	27.8	44.2	-136.8	-120.3	96.0	77.5	30.2	30.3
RK5	5.8	-122.8	147.5	-13.8	63.9	-148.6	-148.3	151.2	146.3	54.1	54.6
RK6	6.0	-135.7	153.1	-2.3	80.3	-156.1	-146.1	119.9	117.3	56.7	57.5
RK7	5.0	-144.7	160.2	-11.7	53.9	-134.4	-120.2	145.0	136.2	58.3	57.8
RK8	5.4	-117.9	133.6	-5.3	45.5	-124.6	-115.5	131.1	130.0	43.9	44.8
Flat Areas											
FT1	5.9	-23.7	24.4	-1.1	7.9	-22.3	-21.4	24.8	23.2	7.3	7.3
FT2	6.6	-15.7	15.7	0.3	5.6	-15.7	-13.9	14.8	13.1	5.2	5.2
FT3	5.9	-16.7	20.8	0.1	6.6	-17.8	-17.0	20.0	19.8	6.4	6.3
FT4	6.2	-11.3	18.8	1.4	5.4	-12.5	-12.5	17.3	16.3	5.2	5.2
FT5	8.6	-28.1	26.8	-1.5	9.3	-26.5	-26.5	27.7	24.5	7.7	7.8
FT6	8.6	-15.8	26.0	-2.7	6.9	-11.8	-10.7	28.4	23.8	4.6	4.5
FT7	7.7	-28.7	13.1	-5.9	8.2	-23.8	-20.8	16.8	15.9	6.3	6.3
FT8	8.9	-30.2	24.0	-3.7	7.8	-26.3	-20.4	26.1	21.6	6.6	6.7
Marine Areas											
MR1	3.0	-33.4	31.2	-0.9	58	-32.6	-30.1	-30.1	31.2	31.2	7.2
MR2	3.1	-189.1	144.0	-2.7	439	-184.1	-188.9	-188.9	116.1	116.1	24.2
MR3	4.6	-39.1	68.0	5.2	266	-49.4	-49.2	-49.2	64.0	64.0	12.6

Since the frequency domain method requires that data be given on a regular grid, it is necessary to have the gravity data at some specified points. The interpolation of reduced gravity anomalies is carried out by the Suffer software using ordinary Kriging (Blais, 1982). Predicting gravity data by collocation method (Moritz, 1980) was not employed in

the gridding procedure due to the amount of computation involved. Tables 4.2 and 4.3 present the statistics of the reduced and free-air gravity anomalies before and after gridding, respectively. The average inter point distance (IPD) represent the actual data resolution before gridding, and it is estimated as

$$\mathrm{IPD} = \frac{\mathrm{NP}}{\sqrt{\mathrm{A}}} \tag{4.1}$$

where NP represents the number of data point in the selected block area, and A is the area size. It should be noted that the gravity anomalies are also centered after gridding by subtracting the mean value from the data.

Table 4.3: Statistics of free air gravity anomalies before and after gridding

(all values are in mGal)

Test Area	**Before Gridding**				**After centering (mean = 0) and gridding with 1′ spacing**		
	Min	**Max**	**Mean**	**Std**	**Min**	**Max**	**Std**
RK1	-71.3	53.9	-7.7	28.7	-69.9	59.6	22.3
RK2	-81.5	70.3	4.2	27.6	-88.0	63.5	17.8
RK3	-107.0	66.5	-8.9	39.4	-101.9	63.8	28.4
RK4	-122.9	90.1	16.4	40.1	-136.1	70.3	27.9
RK5	-136.9	117.6	-23.3	61.2	-144.2	128.6	51.3
RK6	-154.9	109.7	-19.0	5756	-155.3	97.9	2833
RK7	-184.9	126.3	-19.6	2616	-161.2	126.7	2667
RK8	-137.3	92.0	-11.0	1616	-134.2	100.0	1385

4.2 ESTIMATION OF COVARIANCE FUNCTION PARAMETERS

The essential parameters (C_0 and $\chi_{1/2}$) are estimated for each of the test areas. The C_0 value is derived from the following equation

$$C_0 = \frac{1}{n}\sum_{i=1}^{n} \Delta g_i^2 \qquad (4.1)$$

where n is the number of gravity observations in the test area. In order to obtain $\div_{1/2}$, the covariance values at a 1′ spherical distance interval are first derived. Then a fifth order polynomial function is fitted to the covariance functions. The $\div_{1/2}$ values are estimated from the fitted polynomial function by an iterative procedure.

4.3 RESULT AND DISCUSSION

The results of the empirical covariance functions of the gravity anomalies using the space domain method and spectral method for each of the selected areas are presented in this section. In addition, the characteristics of the local covariance functions are discussed.

The empirical covariance function is estimated in the space domain using equation (3.7) with $\Delta\psi = 1$ arcmin. The results of the space domain empirical covariance functions are fitted to the model in equation (3.16) with the degree variance model derived from the Tscherning/Rapp model.

Empirical non-isotropic 2D covariance functions are estimated from the 2D PSDs with equation (3.11), which is evaluated via FFT. To minimize the effect of circular convolution (Sideris, 1994), 100% zero padding is used. The 1D isotropic covariance functions are derived from the corresponding 2D covariance functions by averaging over the azimuths with equation (3.12).

Figures 4.2, 4.3 and 4.4 show the graphs of the results of the space domain (SPC) and frequency domain (FFT) methods alongside with the plots of the corresponding covariance function model (MDL) obtained after fitting the result of the space domain method to the covariance model. The results of the space domain method show oscillations, which are more pronounced in some distance intervals. These oscillations are due to few data points available for the distance interval.

Each figure (4.2, 4.3 and 4.4) shows the 1D isotropic (upper graph) and 2D non-isotropic (lower graph) covariance function for an area in the mountainous (RK6), flat (FT2) and marine (MR3) test areas, respectively. Tables 4.4 and 4.5 present the statistics of the variances C_o and correlation distance $\chi_{1/2}$ estimated with both space domain and Fourier transform methods for all the selected areas.

In the mountainous areas (Table 4.4), the value of C_o varies between 980mGal^2 and 7000mGal^2 for the space domain method after fitting with a model while the corresponding value for the frequency domain method is much lower than expected and varies between 420mGal^2 and 3300mGal^2. Estimates of the correlation distance for the space domain method vary between 2.6′ and 4.0′ while those of the frequency domain method vary between 3.9′ and 6.5′.

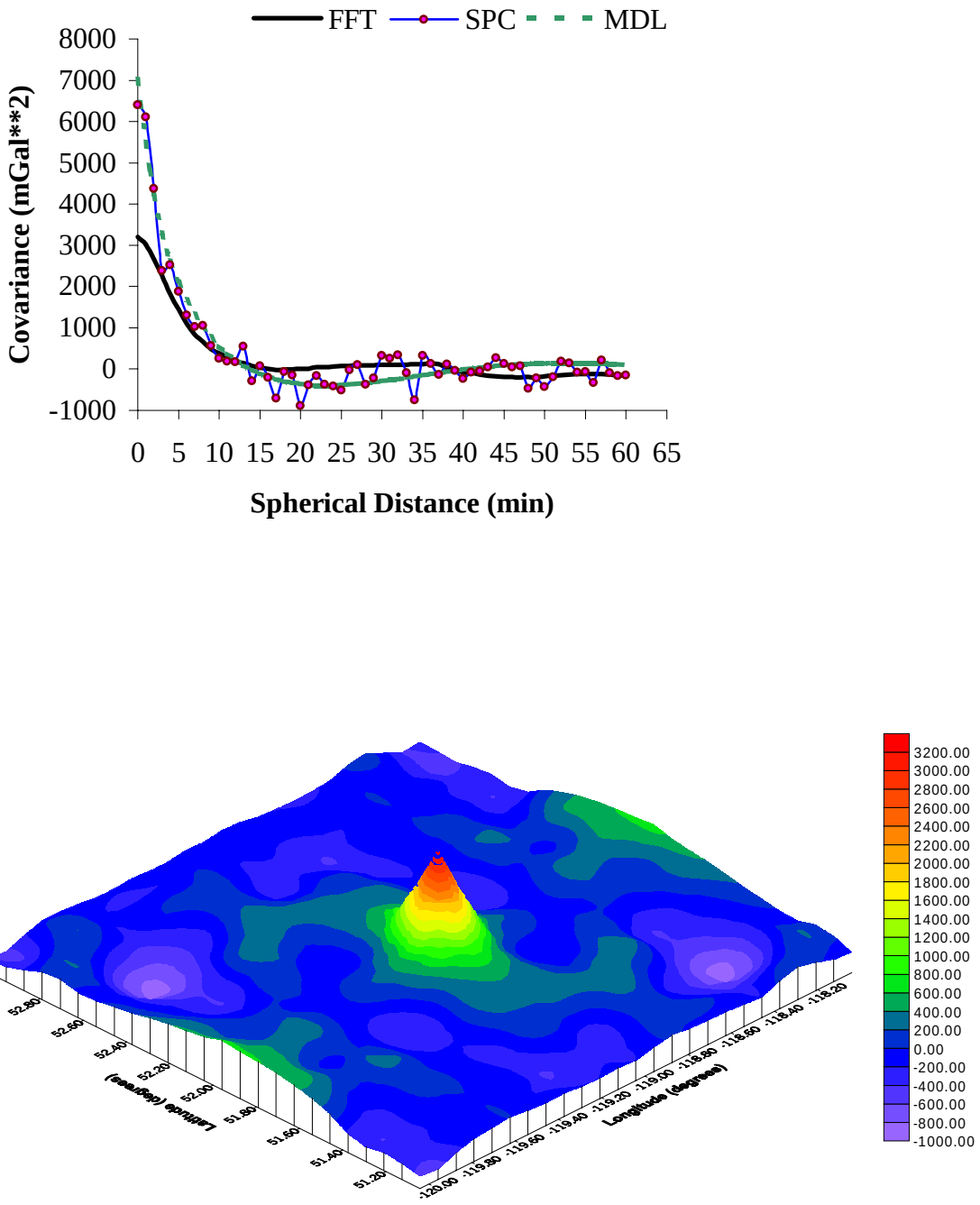

Figure 4.2: Empirical 1D and 2D gravity anomaly covariance function for a mountainous area (RK6), in $mGal^2$

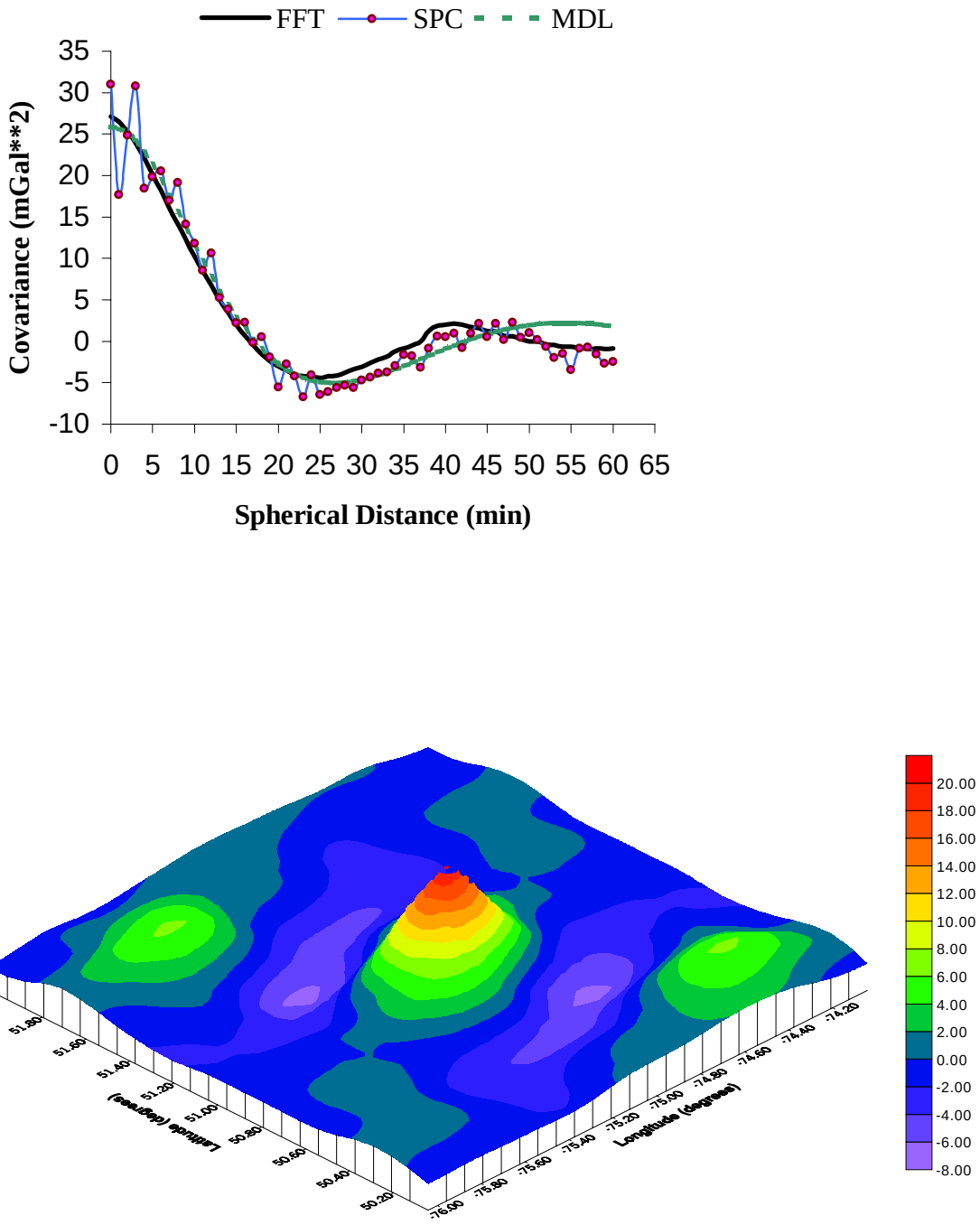

Figure 4.3: Empirical 1D and 2D gravity anomaly covariance function for a flat area (FT2), in $mGal^2$

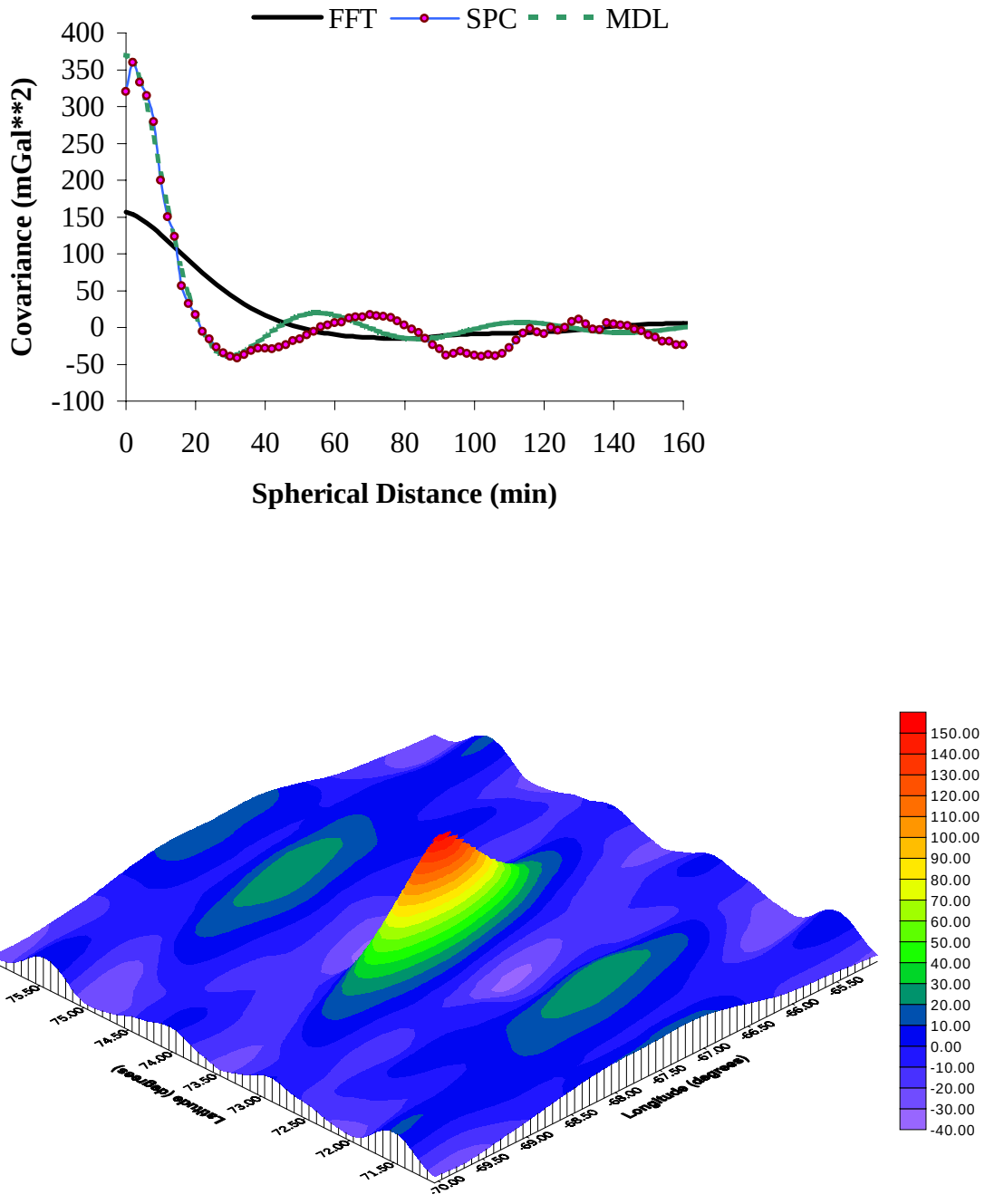

Figure 4.4: Empirical 1D and 2D gravity anomaly covariance function for a marine area (MR3), in mGal^2

Table 4.4: Gravity anomaly covariance function parameters for mountainous areas

Test Area	Frequency Domain Method				Space domain method	
	5′ Spacing		1′ Spacing			
	C_o (mGal^2)	χ (′)	C_o (mGal^2)	χ (′)	C_o (mGal^2)	χ (′)
RK1	646	5.6	622	5.6	984	3.5
RK2	417	3.9	404	3.9	1012	2.9
RK3	1028	4.2	997	4.3	2606	3.3
RK4	915	4.6	914	4.6	1646	3.3
RK5	2976	4.6	2924	4.8	3882	2.6
RK6	3311	4.5	3211	4.6	7026	3.2
RK7	3339	6.5	3394	6.2	1675	2.8
RK8	2004	5.7	1924	5.3	2059	4.0

The results of the space and frequency domain methods for the flat and marine areas (Table 4.5) are however close with little change in the variance values and correlation distances. For flat areas, estimates of the variance vary between 20mGal^2 and 60mGal^2 for the frequency domain method and 26mGal^2 and 90mGal^2 for the space domain method. The correlation distance varies between 7.3′ and 9.4′ for the frequency method while the space domain method estimates vary between 5.2′ and 8.3′. The results for the marine areas show that the variance values vary widely from one area to the other; the correlation length is between 7.0′ and 10.6′, and 8.1′ and 9.4′ for the frequency and space domain methods, respectively.

The results of the covariance function parameters estimated by frequency domain method for referenced free air gravity anomalies in the mountainous areas are presented in Table 4.6.

Table 4.5: Gravity anomaly covariance function parameters for flat and marine areas

Test Area	Frequency Domain				Space Domain	
	5′ Spacing		1′ Spacing			
	C_o (mGal^2)	χ (′)	C_o (mGal^2)	χ (′)	C_o (mGal^2)	χ (′)
Flat Areas						
FL1	54	8.4	54	7.4	56	8.2
FL2	27	8.4	27	5.2	26	7.7
FL3	40	9.4	41	6.4	28	8.3
FL4	27	8.3	27	5.2	27	6.4
FL5	60	8.4	59	7.7	86	5.8
FL6	20	7.3	21	4.6	51	6.1
FL7	40	7.8	40	6.3	82	8.3
FL8	44	7.6	44	6.6	55	5.2
Marine Areas						
MR1	52	7.0	52	7.0	74	8.1
MR2	423	7.9	415	7.6	342	8.8
MR3	159	10.6	157	10.5	370	9.4

Table 4.6: Free air gravity anomaly covariance function parameters

Test Area	RK1	RK2	RK3	RK4	RK5	RK6	RK7	RK8
C_o (mGal^2)	491	309	792	770	2627	2833	2667	1384
χ (′)	5.6	3.1	4.3	4.7	4.7	4.5	5.7	4.8
κ	1.4	1.8	2.7	1.7	2.4	2.0	2.2	1.7

The results presented in Figures 4.2 to 4.4 and Tables 4.4 and 4.5 show that covariance functions estimated by both the frequency and space domain methods vary for the different areas selected. In the mountainous areas, the covariance functions have higher variance value and shorter correlation distance when compared to the corresponding

values estimated for the flat and marine areas. It should be noted that both the frequency and space domain methods are influenced by 'smoothing' effect, due on the one hand to the gridding procedure employed in the frequency method an on the other hand to the azimuth averaging employed in the space domain method. The smoothing effect depends to a great extent on the roughness of the topography and the distribution of the data points in the local area. The data distribution is represented by the average inter-point distance (IPD), which is given in Tables 4.4 and 4.5. The lower the IPD value with better data distribution, the less the smoothing effect.

In areas with rather flat topography, the empirical covariance function functions from both space and frequency domain methods agree better in most of the test areas; for areas with very rough topography, the covariance function from the space domain method and frequency domain method vary widely. Again this can be attributed to the 'smoothing effects' which is more pronounced for areas with rough topography.

The effect of the grid spacing on the covariance estimates is shown in Tables 4.4 and 4.5. Using the frequency domain method with data on 5′ and 1′ grid, the covariance function estimates have smaller variance value and the correlation distance with the 1′ grid data when compared with the corresponding results for 5′ grid data.

CHAPTER 5

HIGH FREQUENCY VARIATION OF THE GRAVITY FIELD SIGNAL SPECTRUM, AND ESTIMATION OF REQUIRED SAMPLING DENSITY FOR LOCAL GRAVITY DATA

In this chapter, analysis of the spectrum of the gravity field signals is discussed. Information from the spectrum of the gravity field data is used to derive among other things the decay parameters for different frequency bands of the gravity field signal spectrum, and estimate the sampling density for local gravity data and heights required to provide a certain geoid accuracy and resolution.

The very high frequency information of the local gravity field is derived from very dense digital elevation model data (DEM) on a 3″×3″ grid while local gravity anomalies on a 1′×1′ grid are used to derive the medium to high frequency gravity field information. The long wavelength information characteristics of the gravity field are determined from the EGM96 geopotential model.

The spectrum of the geoid from various gravity field signals for a selected area is first presented in section 5.1; the geoid spectrum from EGM96 and local gravity data is analyzed in view of the combination of GM and gravity data. In section 5.2, the results of estimated geoid degree variances for selected areas are presented alongside the derived variances from the Tscherning/Rapp model and degree variances with decay implied by the Kaula rule for comparison. In addition, estimates of the decay parameter for the test areas are presented. Section 5.3 discusses gravity data resolution requirement for various levels of geoid accuracy in the centimetre to decimetre range.

5.1 GEOID SPECTRUM FROM GM, LOCAL GRAVITY DATA AND TOPOGRAPHIC HEIGHTS

In this section, the power spectrum of the geoid represented by the degree variances σ_N^2 (in cm^2), is estimated for the various local geoid components. The GM geoid degree variances are given as

$$\sigma^2_{N_{GM}} = \frac{(GM)^2}{\tilde{a}^2 R^2} \sum_{m=0}^{n} \left(\bar{c}^2_{nm} + \bar{s}^2_{nm} \right) \tag{5.1}$$

while the geoid degree variances from gravity anomaly and terrain corrections is derived from

$$\sigma^2_{N_{\Delta g}} = \frac{\sigma_n^2}{\tilde{a}^2} \tag{5.2}$$

where σ_n^2 is derived from equation (3.23).

Global degree variance models given by the Kaula's rule (Kaula, 1966) and the Tscherning/Rapp model (Tscherning and Rapp, 1974) are also employed herein for comparison. The Kaula's rule is given as

$$\sigma_n^2 \approx 0.7 \times 10^{-10} \frac{2n+1}{n^4} \tag{5.3}$$

The Tscherning/Rapp model for Bjerhammar sphere depth $(R_B - R_E = 1.2\text{km})$ is given as

$$\sigma_n^2 \approx 4.4\times10^{-10}\,\frac{0.99962^{n+1}}{(n-1)(n-2)(n+24)} \qquad (5.4)$$

The results of the geoid power spectrum derived from, the EGM96 (GM_NVAR) complete to degree and other 360, the local gravity data (GV_NVAR), the terrain correction (TC_NVAR), and the geoid indirect effect (IND_VAR) are shown in Figure 5.1. The data sets used for the analysis are selected from an area block of 15°×15°, which is located in the Alberta and British Columbia provinces between latitudes 50.0471 and 65.0471, and longitudes -128.0471 and -113.047. The selected area is similar to the one used for GM and local gravity combination analysis in chapter two of this thesis. The statistics of the data sets are given in Table 2.1. The resolution of the local gravity data is 5′×5′, while the DEM data are interpolated on 5′×5′ grid.

Figure 5.1 shows the importance of proper modeling for all local terrain effects on the geoid undulation signal especially in mountainous areas. Terrain correction alone can create a geoid signal which amounts to over 10 cm (rms) for harmonic degree $n < 2{,}150$. The corresponding value for flat areas (Kotsakis and Sideris, 1998) show that such topographic effects should always be taken into account if a centimetre geoid is truly desired.

It is also interesting to note (Figure 5.1) the significant amount of low-wavelength power that the geoid indirect effect signal appears to have for harmonic degrees n > (~320) in the selected area. It completely dominates over the geoid signal originating from the use of the terrain correction. In particular, the geoid indirect effect shows a rms value of approximately 1.8 cm inside the spectral band 24 < n < 2,150, while the geoid component from the terrain correction in the same band has an average power of 10.3 cm. The local

free-air geoid also has a signal power at the 4.5 cm level over the spectral band 360 < n < 2,150; the geoid rms power from terrain correction and geoid indirect in the same spectral band are 0.3 cm and 0.7 cm, respectively. All the corresponding values in the spectral band 360 < n < 2,150, for flat test areas (Kotsakis and Sideris, 1998) are almost negligible. The effect of using local gravity data in lager cap size for geoid estimation is again shown in Figure 5.1. A closer look of the geoid spectrum form EGM96 and local gravity data is shown in Figure 5.2.

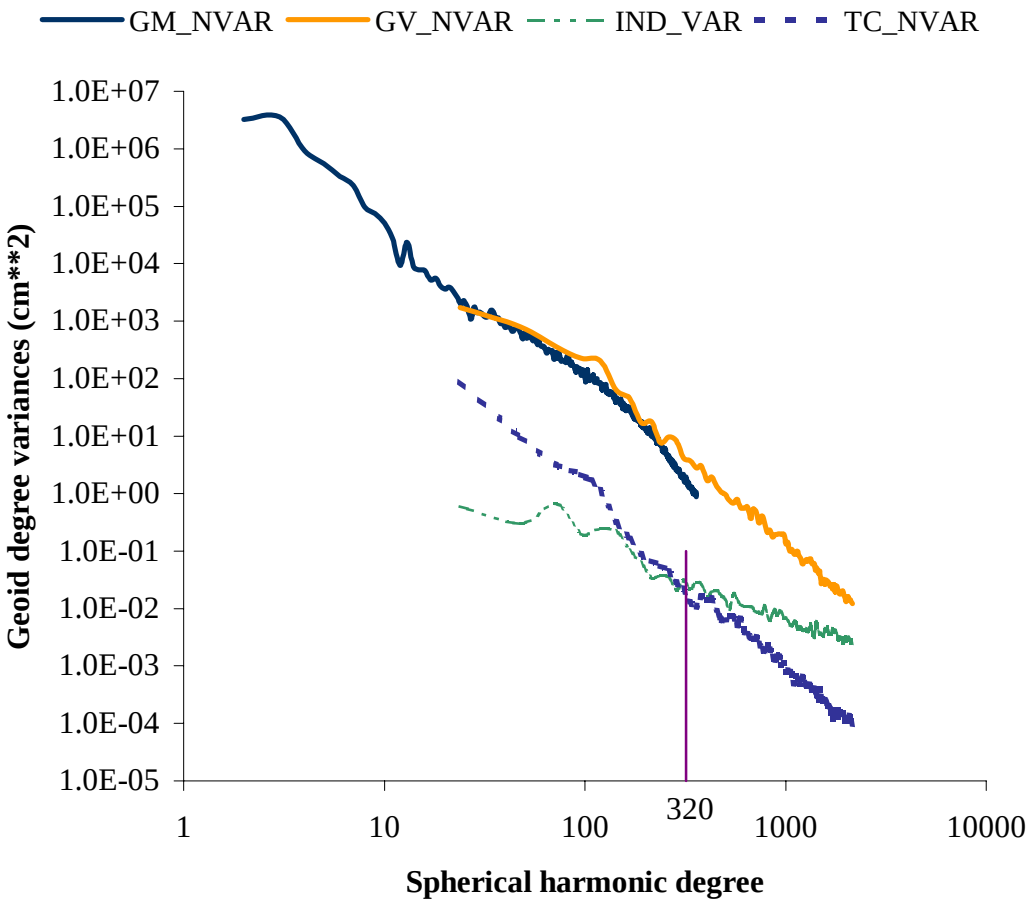

Figure 5.1: Geoid power spectrum from various gravity field signals

In Figure 5.2, the vertical lines represent the cap sizes containing the local gravity data. As shown in Figure 5.2, the power from local gravity data (GV_NVAR) is higher than that from the EGM96 (GM_NVAR) for frequencies higher than that corresponding to a cap size of 10°×10°. Below the frequency that corresponds to a 10°×10° cap size, the geoid power spectrum is dominated by the contribution from EGM96. It is also evident that when a cap size of 1 degree, which corresponds to 360 harmonic degree, is used the contribution from the local gravity data will not provide all the necessary information required for accurate geoid determination.

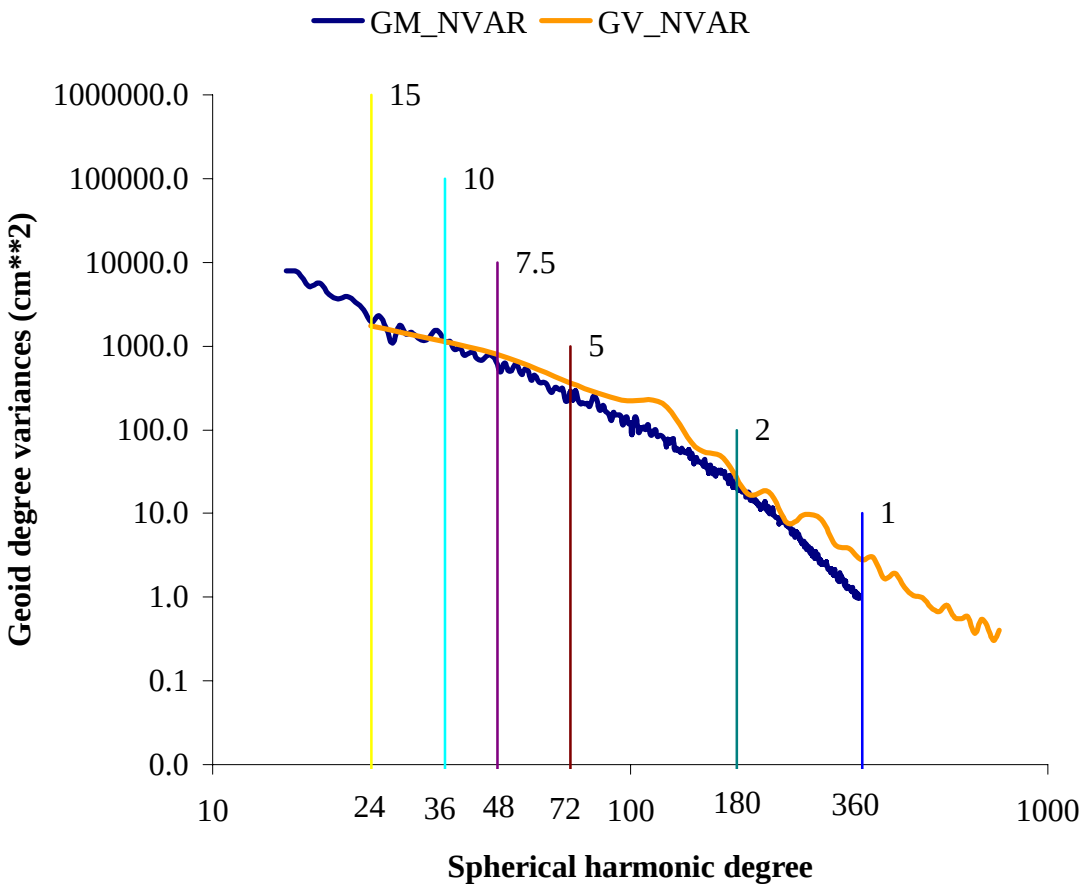

Figure 5.2: Geoid power spectrum from EGM96 and local gravity data

5.2 THE DECAY OF THE GRAVITY FIELD SPECTRUM IN THE HIGH WAVE NUMBERS

This section discusses the variation of the earth gravity field spectrum in medium and high frequencies, and the results of the estimates of the decay parameters for local areas are presented.

On a global scale, the earth gravity field spectrum has been known to obey a power decay law in the form of

$$\sigma_n^2 \approx \frac{\alpha}{n^{\beta}} \qquad (5.5)$$

where α and β are constants. The constant β describes the rate of decay of the gravity field spectrum.

In Figure 5.1, the geoid power spectra originating from the local gravity data and the terrain correction seem to follow a faster decaying pattern than the spectrum of the third geoid component (indirect effect). A comparison of the geoid power σ_N^2, derived from local gravity anomalies, with global models in equations (5.3) and (5.4) is shown in Figures 5.3, 5.4 and 5.5, respectively for mountainous, flat and marine test areas in Canada. The test areas and gravity data are similar to those used for covariance analysis in chapter four of this thesis. The location of these areas is shown in Figure 4.1 while the statistics of the gravity and height data are given in Tables 4.2 and 4.1, respectively.

Each figure (5.3, 5.4 and 5.5), shows the plot of the estimated geoid degree variances (DEGV) from local gravity anomalies alongside the plot of the Tscherning/Rapp degree variance (TRMDL) and degree variance with decay implies by Kaula rule (KMDL). The result of using linear models fitted to the estimated degree variance (MDL) is also shown in these figures. All the graphs are shown on logarithmic scale. The 1′×1′ gridded gravity anomalies used for estimating $\acute{o}_N^2$ provide a maximum harmonic degree of 10,800. The minimum recoverable degree for flat and mountainous areas is 180 while that of the marine areas is 72, since the area size is $2^o \times 2^o$ and $5^o \times 5^o$ for flat/mountainous and marine areas, respectively.

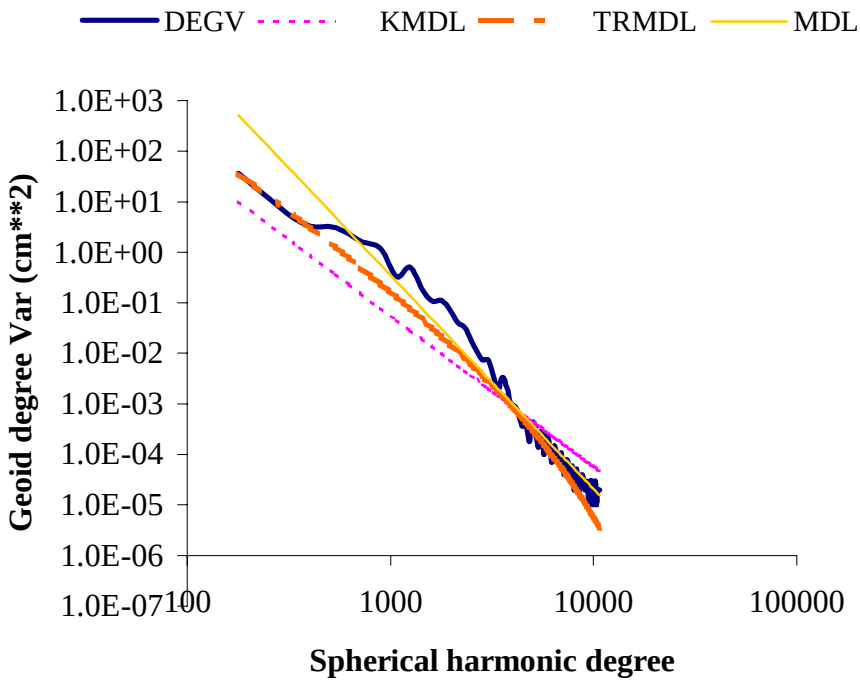

Figure 5.3: Geoid degree variances for a mountainous (RK6) area

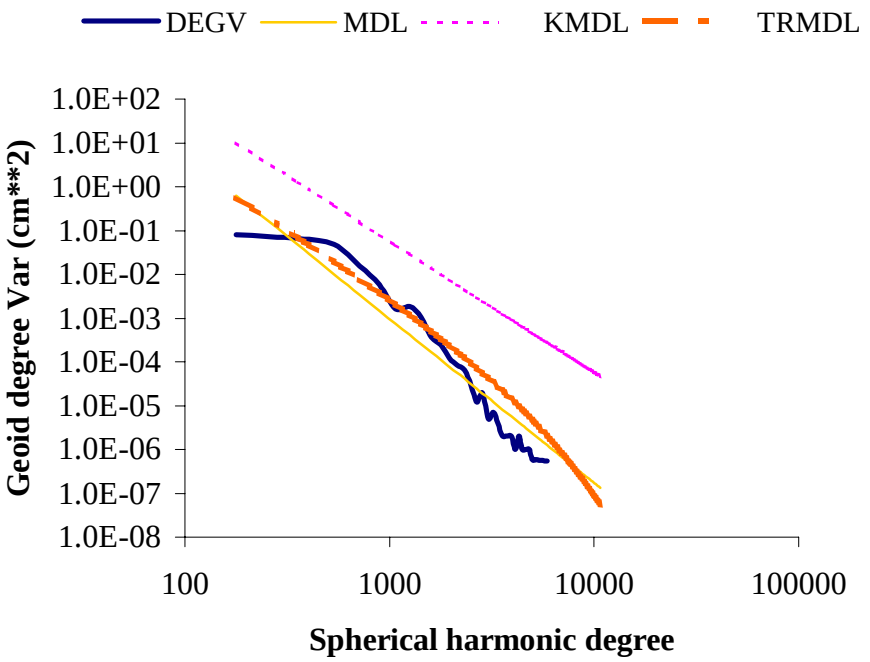

Figure 5.4: Geoid degree variances for a flat (FT2) area

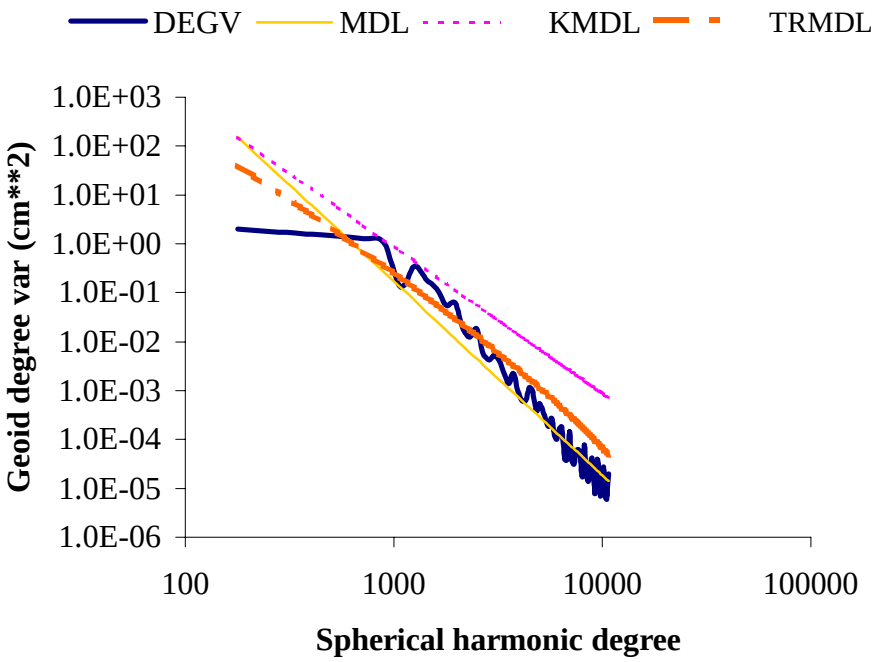

Figure 5.5: Geoid degree variances for a marine (MR3) area

The values of the parameters á and â in equation (5.5) are estimated for various bands of the harmonic degree by least-squares fittings of a linear model to the estimated values. Tables 5.1 and 5.2 show the results of the constants á and â for all selected areas in mountainous, and flat and marine areas of Canada, respectively.

Table 5.1: Local geoid decay parameters at various spectral bands for mountainous areas

Test Area	**Band Range**			
	$180 \le n \le 3030$		$3030 \le n \le 10800$	
	á	â	á	â
RK1	-8.6	-3.4	-5.2	-4.5
RK2	-11.0	-2.8	-4.5	-4.7
RK3	-9.6	-3.0	-4.2	-4.7
RK4	-9.7	-3.0	-2.9	-5.0
RK5	-10.0	-2.9	-4.0	-4.6
RK6	-9.0	-3.0	-4.2	-4.6
RK7	-7.6	-3.5	-4.8	-4.5
RK8	-8.5	-3.3	-5.2	-4.5
Mean		**-3.2**		**-4.6**

In Figures 5.3 to 5.5, the geoid spectra originating from the local gravity data seem to follow a faster decaying pattern than the Kaula rule implies (5.3), especially in the spectral band above n = 3030 (Tables 5.1 and 5.2). These result agree with similar indications given in previous studies in Canada (Kotsakis and Sideris, 1998; Vassiliou and Schwarz, 1985) and in northern Europe (Forsberg, 1986). The spectral decaying pattern for geoid (from local gravity data) is in good agreement with the Tscherning/Rapp model (Figures 5.3, 5.4 and 5.5) and EGM96 geoid degree variances (Figure 5.1 and 5.2), in the spectral

band 60 < n < 360. In addition, the local geoid spectra decay faster in high frequencies (n > 3030) with â > 4.0 for most areas.

Table 5.2: Local geoid decay parameters at various spectral bands for flat and marine areas

a) Flat

Test Area	**Band Range**			
	$180 \le n \le 3030$		$3030 \le n \le 10800$	
	á	â	á	â
FT1	-7.9	-4.1	-9.0	-3.9
FT2	-9.6	-3.6	-9.4	-3.8
FT3	-8.8	-3.8	-8.1	-4.2
FT4	-8.3	-4.0	-9.3	-3.8
FT5	-7.8	-4.1	-8.3	-4.1
FT6	-9.9	-3.5	-6.4	-4.3
FT7	-9.2	-3.7	-8.4	-4.1
FT8	-9.5	-3.6	-9.2	-3.8
Mean		**-3.8**		**-4.0**

b) Marine

Test Area	**Band Range**			
	$180 \le n \le 3030$		$3030 \le n \le 10800$	
	á	â	á	â
MR1	-9.8	-3.4	-4.6	-5.0
MR2	-7.2	-4.0	-9.2	-3.5
MR3	-6.6	-4.4	-7.5	-4.2

5.3 DATA RESOLUTION REQUIREMENT FOR GEOID ESTIMATION

In order to investigate the required data spatial resolution for certain level of geoid accuracy, gravity data and topographic heights in both the mountainous and flat areas are analyzed separately in view of the wide difference in the gravity field signals in both areas (Table 4.2). In this section, the estimation of spatial resolution for local gravity data and heights required for centimetre to decimetre geoid accuracy in the mountainous and flat areas of Canada is presented.

The contribution of the local gravity field data to the geoid can be investigated from estimates of the geoid short wavelength power. The estimated geoid short wavelength power contains the rms value of the local geoid signal contributed above a certain harmonic degree n_o, and can be expressed as

$$\sigma_N^2(n > n_o) = \frac{1}{\tilde{a}^2} \sum_{n>n_o}^{\infty} \sigma_n^2 \qquad (5.6)$$

where $\sigma_N^2(n > n_o)$ represent the geoid rms value above certain spherical harmonic degree.

The estimated values of σ_N^2 for different n_o, which correspond to the highest harmonic degree and consequently to the data spacing, provides a means of evaluating the data resolution requirement for the decimetre to centimetre geoid accuracy. It should be noted that the values of σ_N^2 represent only the ideal local geoid variance, since in most cases the spherical harmonics errors of the reference field will be much larger than these values.

The graph of estimates of σ_N^2 derived from gravity data and fitted models in the selected mountainous and flat test areas of Canada against n_o are shown in Figure 5.6. The corresponding results after adding the effect of the topography are shown in Figure 5.7. In estimating σ_N^2, it is assumed that a perfect (linear) correlation exists among all the geoid components. The plotted geoid rms values are based on the average of σ_N^2 estimates for the mountainous test areas and flat test areas.

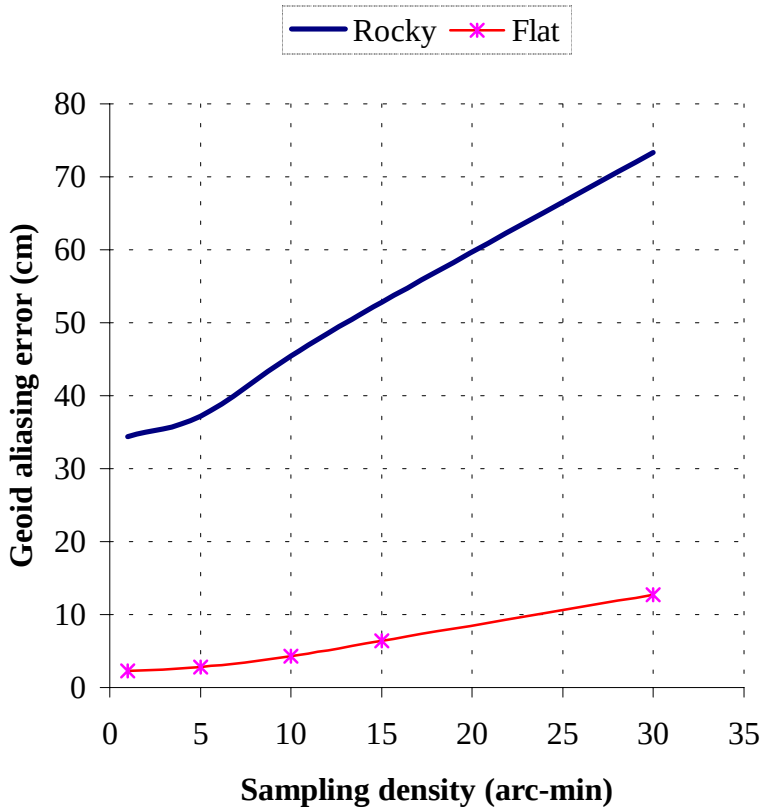

Figure 5.6: Local data sampling density for cm-dm geoid without topographic effect

As shown in Figures 5.6 and 5.7, the use of very dense local gravity data (e.g., 1′×1′) in mountainous areas will result in a geoid accuracy at the 30-35 cm level, while the incorporation of equally dense height data will bring the accuracy down to the 2-3 cm level. On the other hand, the required gravity and height data resolution in the same areas for cm-geoid was estimated to be 0.5′ and for dm-geoid 7′-7.5′.

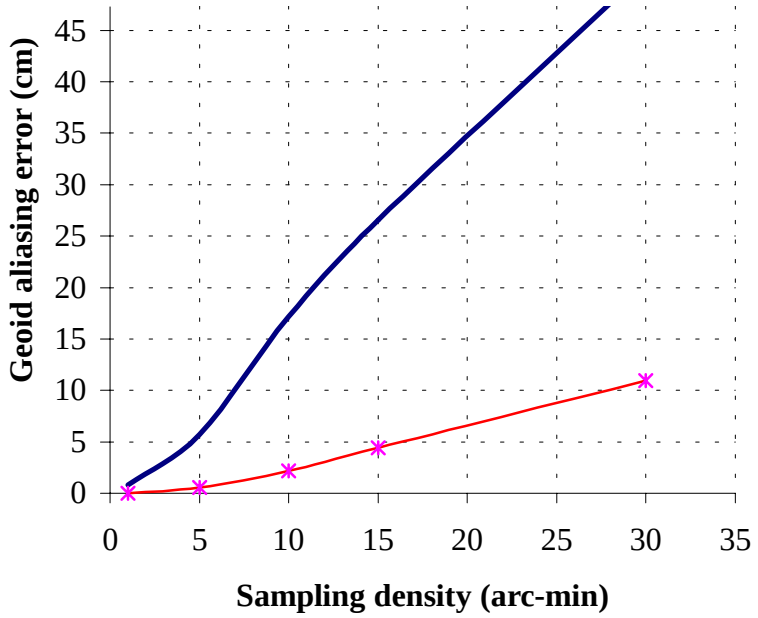

Figure 5.7: Local data sampling density for cm-dm geoid with topographic effect

In the flat areas of Canada, dm-geoid accuracy can be achieved without even taking terrain effects into account, by using a local gravity grid spacing of 20′. For cm-level geoid, gravity and terrain data should be combined with a resolution better than 6′. It should be noted that all the above accuracy estimates refer to an average spatial behavior and individual point errors may vary from these values.

CHAPTER 6

ANALYSIS AND MODELLING OF THE GEOID ERRORS

In geoid determination, a number of error sources limit the accuracy of the predicted geoid undulations. The most significant of these errors are due to the noisy data used in the conventional geoid estimation: the geopotential model (GM), local gravity anomalies Δg and the heights. Smaller errors due to datum biases, spherical approximation, and the mass of the atmosphere are usually considered to be at the noise level (Sideris and Schwarz, 1986), and are not taken into consideration in this study; further details about this class of errors can be found in Heiskanen and Moritz (1967).

The two basic methods that are used to evaluate the accuracy of gravimetrically derived geoid undulations, external comparison with GPS/levelling benchmarks and internal propagation of data errors, are employed in the estimation of the geoid error covariance functions. The methodology for the internal error propagation is similar to that employed by Sideris and Schwarz (1986 and 1987). Absolute geoid error covariances from each source are derived by propagation of error covariances of the data source.

Covariance models for relative geoid errors can be derived by propagating the error covariances of absolute geoid for two baselines. Then the contribution of each data to the relative geoid error variances and covariances can be investigated as for the absolute geoid undulation error covariances, which is presented in the sequel. Derivation of the expressions for the relative geoid error covariance function is contained in Sideris and Schwarz (1986).

In section 6.1, the general expression for geoid error covariance propagation is presented. This is followed by error covariance models from the GM coefficients, gravity data and heights, which are presented in section 6.2. In sections 6.3 and 6.4, estimates of the errors from GM coefficients and gravity data are derived for two areas selected, respectively. Section 6.5 presents the results of the combined geoid error covariance function from both GM and gravity data are discussed. In addition, estimates of the geoid errors derived from comparison of gravimetric geoid and GPS/levelling derived geoid are compared with the internally propagated geoid errors from the GM and local gravity data.

6.1 DATA ERROR PROPAGATION

Applying the theory of error propagation to the expression for geoid estimation in equation (2.1), the error variance of the geoid undulations, under the assumption of uncorrelated data errors, can be expressed as

$$\acute{o}^2_{N_T} = \acute{o}^2_{N_{\Delta g}} + \acute{o}^2_{N_{GM}} + \acute{o}^2_{N_C} \qquad (6.1)$$

where $\acute{o}^2_{N_T}$ is the combined geoid error variance, $\acute{o}^2_{N_{\Delta g}}$ is the geoid error variance due to error in gravity anomaly, $\acute{o}^2_{N_{GM}}$ is the geoid error variance from the GM, and $\acute{o}^2_{N_C}$ is the geoid error variance due to error in the topographic heights. Again for simplicity, equation (6.1) represents the case where the data errors are assumed to be uncorrelated. The expressions for these components are given (Li and Sideris, 1994) as follows:

$$\acute{o}^2_{N_{\Delta g}} = \left(\frac{R\Delta\varphi\Delta\ddot{e}}{4\pi\tilde{a}}\right)^2 \left(\sigma^2_{\Delta g}\cos^2\varphi + \sigma^2_{\Delta g_{GM}}\right) * \left(S(\psi) - \overline{S}(\psi)\right)^2 \qquad (6.2)$$

$$\sigma^2_{N_{GM}} = R^2 \sum_{n=2}^{360} \sum_{m=0}^{n} (\sigma^2_{\bar{C}_{nm}} + \sigma^2_{\bar{S}_{nm}}) \tag{6.3}$$

$$\sigma^2_{N_C} = \left(\frac{G\rho\pi}{\gamma} \right)^2 \sigma^2_h \tag{6.4}$$

$$\sigma^2_{\Delta g_{GM}} = G^2 \sum_{n=2}^{360} (n-1)^2 \sum_{m=0}^{n} (\sigma^2_{\bar{C}_{nm}} + \sigma^2_{\bar{S}_{nm}}) \tag{6.5}$$

where $\sigma_{\bar{C}_{nm}}, \sigma_{\bar{S}_{nm}}$ are the errors (standard deviations) of the normalized geopotential coefficients of degree n and order m, σ_h is the error (standard deviation) of the height measurement, $S(\psi)$ is the Stokes's Kernel function, and $\bar{S}(\psi)$ is the summation of the Legendre series of Stokes spherical kernel up to n_{max}=360. It is given as, (Li and Sideris, 1994):

$$\bar{S}(\psi) = \sum_{n=2}^{n_{max}} \frac{2n+1}{n-1} P_n(\cos\psi), \tag{6.6}$$

6.2 GEOID ERROR COVARIANCE FUNCTION MODELS

The geoid error covariance function E_N for any data set with geoid error degree variances $\sigma^2_{a_N}$, computed from the data, can be obtained from the following formula, (Sideris and Schwarz, 1986):

$$E_N(\psi_{1:2}) = \mathrm{cov}(\varepsilon_{N_1}, \varepsilon_{N_2}, \psi_{1:2}) = \sum_{n=2}^{n_{max}} \sigma^2_{\delta_N}(N_1, N_2)\, P_n(\cos\psi_{1:2}) \qquad (6.7)$$

where E_N is the error covariance function of the estimated geoid undulation N, $\varepsilon_{N_1}, \varepsilon_{N_2}$ are the errors of the estimated N's of two points at distance $\psi_{1:2}$ apart, $\psi_{1:2}$ is the spherical distance between points 1 and 2, n_{max} is the maximum degree of spherical harmonic expansion, and P_n are the Legendre polynomials.

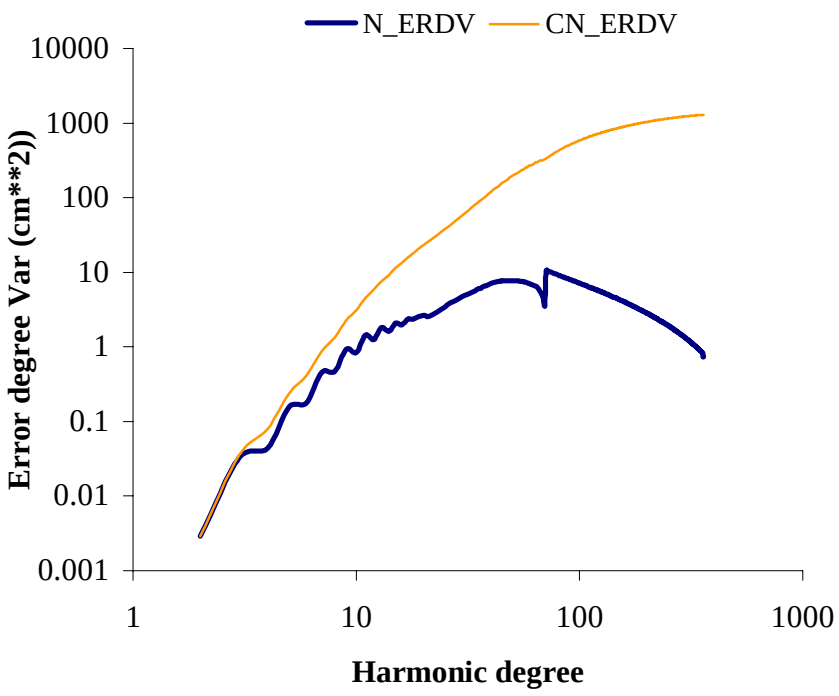

Figure 6.1: Geoid error degree variances of EGM96 coefficients

6.2.1 **GM Coefficients Error Covariance Function**

The geoid error covariance function from the GM coefficients is derived from the error degree variances, which is given in equation (6.3). The graph of the actual (N_ERDV) and cumulative (CN_ERDV) geoid degree variances of the EGM96 geopotential model coefficients plotted against spherical harmonic degree are shown in Figure 6.1. It is evident from Figure 6.1 that the GM geoid errors are more in the long and medium wavelength bands compared to those in the higher frequencies (above 200 harmonic degree). See Pavlis (1997) for detail.

6.2.2 **Estimation and Modelling of Gravity Data Error Covariance Function**

In gravity field prediction by collocation or input output system theory (IOST) using heterogeous data, the overal accuracy of the predicted quantity will depend on how the error information which is contained in the error covariance or PSD function of each data represent the reality for the local area. Well represented error covariance and PSD functions will provide proper weights for the different data and thus improve the precision of the prediction. In this study, an attempt is made to estimate and compare gravity error covariance functions for two areas with different topographic features. This is necessary especially when gravity field prediction is done in areas with diverse topography.

6.2.2.1 Gravity Error Covariance Function Based on Multiple Observations

The error covariance function of local gravity data can easily be derived for areas with multiple gravity databases as documented in Weber and Wenzel (1983) for marine areas. See also Esan and Sideris (1999). However, the availability of multiple gravity data over the terrain surface is practically impossible and thus makes estimation of gravity error

covariance from multiple observations for such areas impossible. In the sequel, gravity errors are obtained by comparing predicted to measured gravity anomalies in the selected areas. The gravity anomalies (Δg) are first corrected for terrain effect and referenced to EGM96. The mathematics of estimating covariance function from multiple observation is presented below.

Assuming a sufficient number of multiple and independent observations of the gravity data, the error covariance function can be estimated from observation differences. Using the parameters g_1, g_2 for true values located at two points separated by a spherical distance ψ_{12}, ℓ for observations, δ for true errors, and the subscripts i, j, k, l for the various data sources, we can write the following expressions:

$$g_1 = \ell_i + \delta_i = \ell_j + \delta_j \qquad g_2 = \ell_k + \delta_k = \ell_l + \delta_l \tag{6.8}$$

Defining the observation differences (dg) as,

$$dg_{1ij} = \ell_i - \ell_j = \delta_j - \delta_i \qquad dg_{2kl} = \ell_k - \ell_l = \delta_l - \delta_k \tag{6.9}$$

the expectation value for product pairs of differences at the two points can be expressed as follows:

$$E\{dg_{1ij} dg_{2kl}\} = E\{\delta_j \delta_l\} - E\{\delta_j \delta_l\} - E\{\delta_j \delta_k\} + E\{\delta_i \delta_k\} \tag{6.10}$$

Equation (6.10) could be estimated as

$$E\{dg_{1ij}dg_{2kl}\} \cong \frac{1}{n}\sum dg_{1ij}dg_{2kl} \qquad (6.11)$$

Replacing expectation values by covariances, we have the following expressions:

$$\frac{1}{n}\sum dg_{1ij}dg_{2kl} \cong \mathrm{cov}(\text{å}_j, \text{å}_l) - \mathrm{cov}(\text{å}_j, \text{å}_k) - \mathrm{cov}(\text{å}_i, \text{å}_l) + \mathrm{cov}(\text{å}_i, \text{å}_k) \qquad (6.12)$$

where n denotes the number of observations in the sources.

Error covariances can be determined in two ways. In the first case, if one of the sources that participated in the evaluation of dg_{1ij} also participated in the evaluation of dg_{2kl} e.g.

$$i = k \qquad j \neq l \qquad (6.13)$$

then using the of hypothesis of zero cross correlation between errors of different sources and inserting equation (6.13) into (6.12), the error covariances for observations of source i can be written as

$$\mathrm{cov}(\text{å}_i, \text{å}_i) \cong \frac{1}{n}\sum dg_{1ij}dg_{2il} \qquad (6.14)$$

In the other case, if both sources that participated in the evaluation of difference dg_{1ij} also participated in the evaluation of the difference dg_{2kl}, then

$$i = k \qquad j = l \qquad (6.15)$$

Accepting the hypothesis of equal error covariances for both sources, and combining equations (6.15) and (6.12), the error covariances is given as

$$\mathrm{cov}(\text{å}_i, \text{å}_i) \cong \frac{1}{2n} \sum dg_{1ij} dg_{2ij} \qquad (6.16)$$

It should be noted that the reliability of the results of these models depend on the validity of the hypothesis introduced. Gravity error covariance functions for the selected areas are computed using equation (6.14). The error degree variances $\text{ó}^2_{n,\Delta g}$ of the gravity anomaly contributed to the undulations are then computed from the corresponding error PSD function with equation (3.23).

The numerical results for two test areas in Canada are shown in Figures 6.2 and 6.3. The two test areas each with $5^o \times 5^o$ block size are located in the west (latitudes 50^o to 55^o, and longitudes -120^o to -115) and in the east (latitudes 46^o to 51^o, and longitudes -74^o to -69^o) of Canada.

The values of parameters characterizing the behavior of the covariance function (the variance C_o and correlation length $\div_{1/2}$) for the two selected areas show that while C_o values are different, the $\div_{1/2}$ values are similar. The variance values are about 318 mGal^2 and 20 mGal^2 respectively for the mountainous and flat areas. Estimated values of $\div_{1/2}$ in the mountainous area is about 4′, while that of the flat area is about 4.5′.

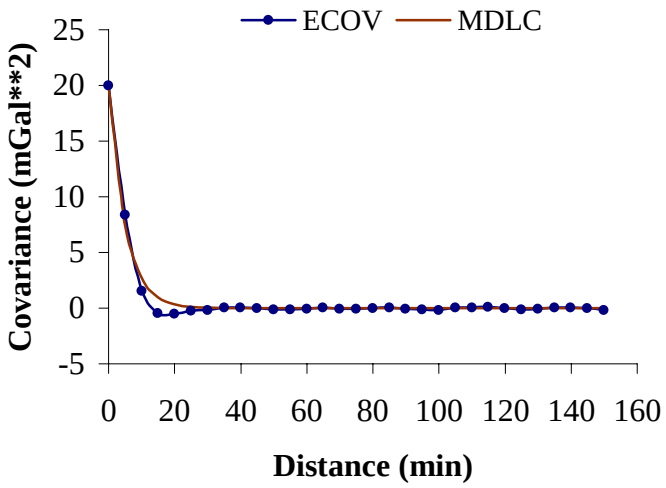

Figure 6.2: Gravity error covariance function for a flat area

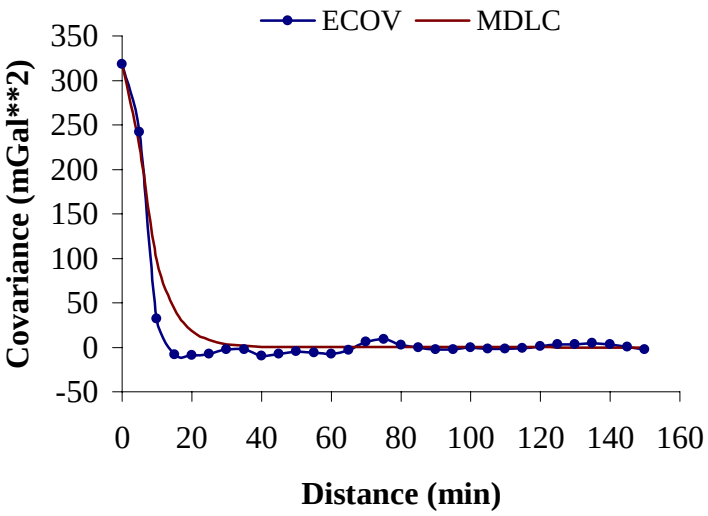

Figure 6.3: Gravity error covariance function for a mountainous area

6.2.2.2 Gravity Error Covariance Function Model

A number of error covariance models for gravity data have been suggested by different authors. Gravity error covariance could be derived from a Gaussian error PSD function $P_{\delta\Delta g}$ (Sideris and Schwarz, 1986), given as

$$P_{\delta\Delta g}(\omega_n) = \frac{a_o}{2a_1^2} e^{-\omega^2/4a_1^2}, \qquad \omega_n = \frac{n+0.5}{R} \tag{6.17}$$

where a_o is a constant with unit (mGal^2) and a_1 is a scaling factor. Both a_o and a_1 are to be determined for each local area. The corresponding covariance function can be written as

$$E_{\Delta g}(\psi_{1:2}) = \mathrm{cov}\{\delta_{\Delta g_1}, \delta_{\Delta g_2}, \psi_{1:2}\} = a_o e^{-a_1^2 \phi_{1:2}^2}, \text{ for } \psi \text{ in degrees.} \tag{6.18}$$

The estimated gravity error covariance model derived after fitting the empirical error covariance values with equation (6.14) is also shown in Figures 6.2 and 6.3 alongside with the empirical covariance values for flat and mountainous areas, respectively. Estimated values of a_o and a_1 of the fitted models are 318.6mGal^2 and 12.0 for the mountainous area, and 20.0mGal^2 and 10.0 for the flat area.

6.2.3 Topographic Effect Error Covariance Model

The effect of the terrain on predicted geoid undulations is very small in areas with smooth terrain, such as in eastern Canada. However, the terrain contribution in areas with rough topography has a considerable effect on predicted gravity field quantities. Error due to the topographic heights can be derived from a Gaussian covariance model given as

$$E_{\Delta g_h}(\psi) = ce^{-d\psi^2}, \text{ for } \psi \text{ in degrees.} \qquad (6.19)$$

where c and d are parameters (with units similar to those of a_1 and a_o) that characterize the behavior of the topographic error effect for the local area. Estimate of c and d for the North American continent is given by Sideris and Schwarz (1986) as 5 $mGal^2$ and 10.5, respectively. To derive estimates of c and d, standard deviations of the gravity observations were propagated into the error variances of the terrain correction equation, and the result modeled using equation (6.19) Geoid error due to the topographic indirect effect can be derived from the corresponding error variances, which is given in equation (6.4), by using equation (6.7).

6.3 GEOID ERROR FROM GM COEFFICIENTS

The evaluation of the error contribution of the GM coefficients can be done with distance dependent data error covariance functions derived from the error degree variances of the GM coefficients. The contribution of the GM errors to $C_N(\psi_{1:2})$ is computed from error degree variances of the EGM96 coefficients with equation (6.3), for which the coefficients

and their errors are given up to degree 360, and the plot of the result is shown in Figure 6.4. The variance value is about 1300cm^2 while the correlation length is about 30′.

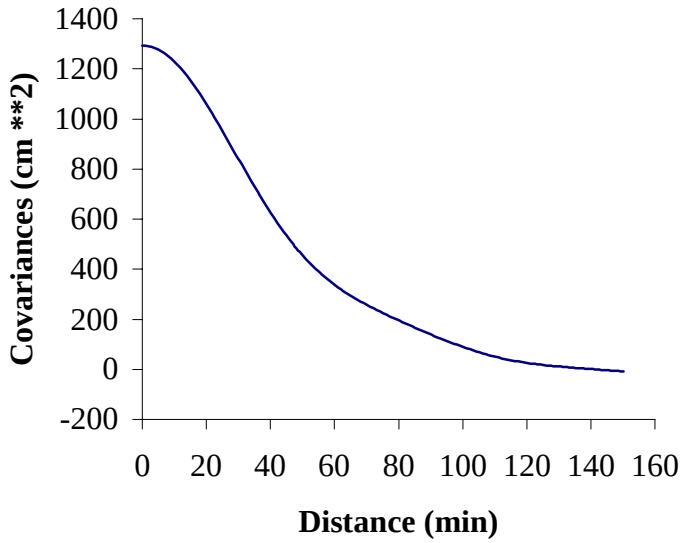

Figure 6.4: Geoid error covariance function from EGM96 coefficients

6.4 GEOID ERROR FROM GRAVITY DATA

Since the gravity anomalies used in the computation of the geoid undulations are referenced to the geopotential model and reduced for topographic effect, the combined gravity error variances is derived for the harmonics of degree $n \le n_{max}$ $(n_{max} = 360)$ from the EGM96 coefficient error using equation (6.5). For $n > n_{max}$, the errors from local gravity data and terrain effect are estimated separately. The local gravity error degree variances is computed as

$$\sigma^2_{n,\Delta g} = \frac{1}{2\pi\gamma^2} \frac{n+\frac{1}{2}}{(n-1)^2} P_{\Delta g \Delta g}(\psi_n), \quad \psi_n = \frac{n+\frac{1}{2}}{R} \tag{6.20}$$

where and n starts at 361, and $P_{\Delta g \Delta g}$ is the isotropic gravity error PSD function estimated from the corresponding error covariance function, which is derived with equation (6.14). The corresponding geoid error covariances computed with equation (6.20) are shown in Figures 6.5 and 6.6, respectively for flat and mountainous test areas.

The variance value of the derived geoid error covariance function is higher for the mountainous test area compared with that from the flat area as expected. In mountainous area, the geoid variance is estimated at about 4.8 cm^2, the corresponding value in the flat area, is about 0.18 cm^2. The correlation length is 7′ for both test areas. Covariance model of the form

$$E_N = a_o e^{-a_1^2 \psi_{1:2}^2} \tag{6.21}$$

is then fitted to the derived covariance values. The values of the parameters a_o and a_1 of the fitted models are estimated as 4.80 cm^2, 6.7 and 0.19 cm^2, 6.3 for the mountainous and flat test areas, respectively.

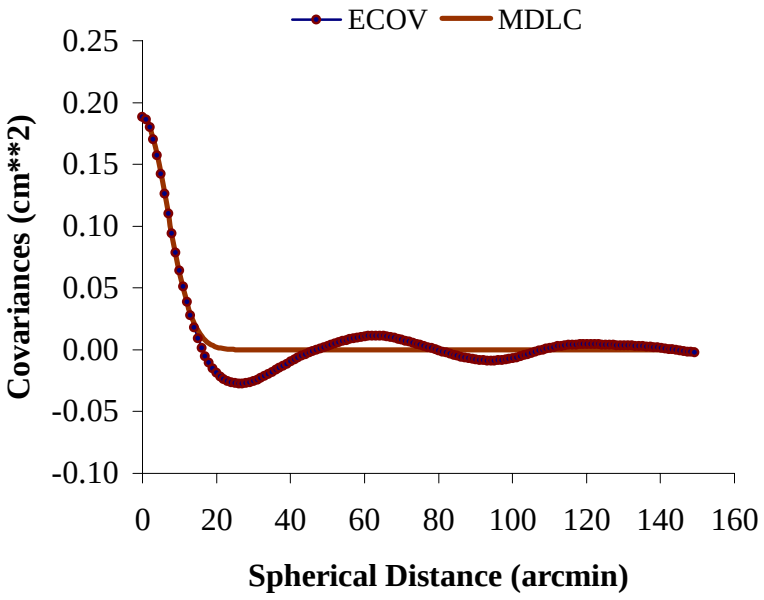

Figure 6.5: Geoid error covariance function from gravity data for a flat area

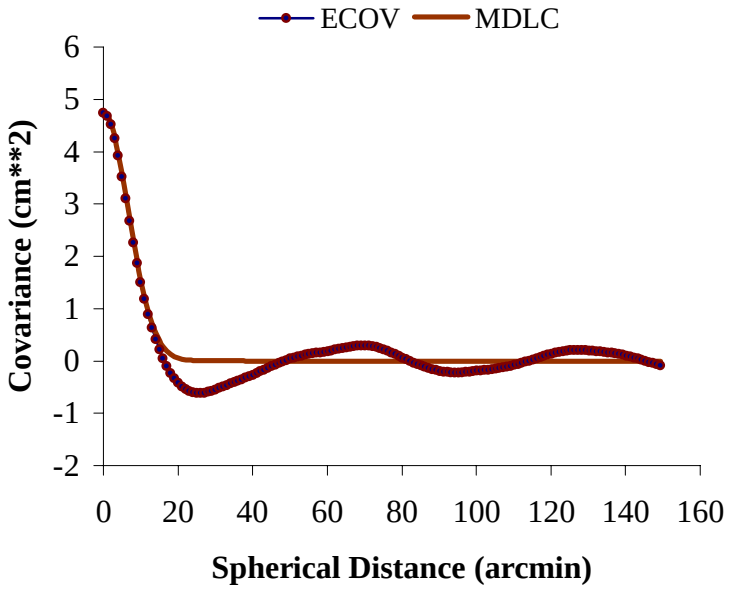

Figure 6.6: Geoid error covariance function from gravity data for a mountainous area

6.5 **Combined Geoid Error Covariance Function**

6.5.1 Geoid Error from GM and Gravity Data

The total geoid error covariance function from gravity and GM is obtained from (6.1) where for $2 \le n \le 360$, the formula (6.4) is used to compute the errors degree variances of the coefficients of the EGM96 geopotential model, for which the coefficients and their errors are given up to degree 360. For $n > 360$, the error covariance functions are computed with equation (6.20). The results for the two selected areas are similar to that shown in Figure 6.2. The variance value for the total geoid error covariance function is about 1300 cm^2 while the correlation length is about 30′ for the two areas. The fact that these values are the same for the two areas is due to the strong influence of the errors coming from the GM which dominates the long and medium wavelength bands of the geoid error spectrum.

6.5.2 Comparison of Internal and External Geoid Errors

Gravimetric geoid undulations are computed for the two selected areas above using the formulas presented in chapter 2. The results of the total geoid were compared to the GPS/leveling data on benchmarks in the two areas (80 and 112 data points for the mountainous and flat areas, respectively). The difference between the gravimetric and GPS/leveling derived geoid provides an estimate of the external geoid error which can be compared to the internal propagated geoid errors. The standard geoid error derived from the difference between the gravimetric geoid and GPS/leveling is about 19 cm and 17 cm for the mountainous and flat areas, respectively.

Covariance functions for the external GPS/leveling derived geoid errors are computed empirically for the two areas and the results are fitted with fourth order polynomial model. The graph of the empirical error covariance functions and fitted models are shown in Figures 6.7 and 6.8 for the flat and mountainous test areas, respectively. Values of fitted model parameters are given in Table 6.1. The covariance function of the external geoid error has a correlation length of about 8′ for the two areas. The variance value of the covariance function for the mountainous area is about 344cm^2 while that of the flat area is about 302cm^2.

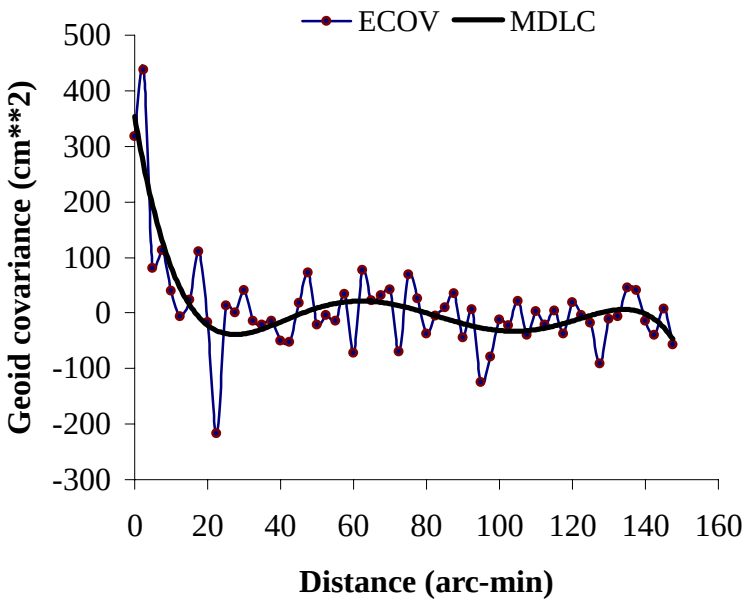

Figure 6.7: GPS/leveling geoid error covariance function for a flat area

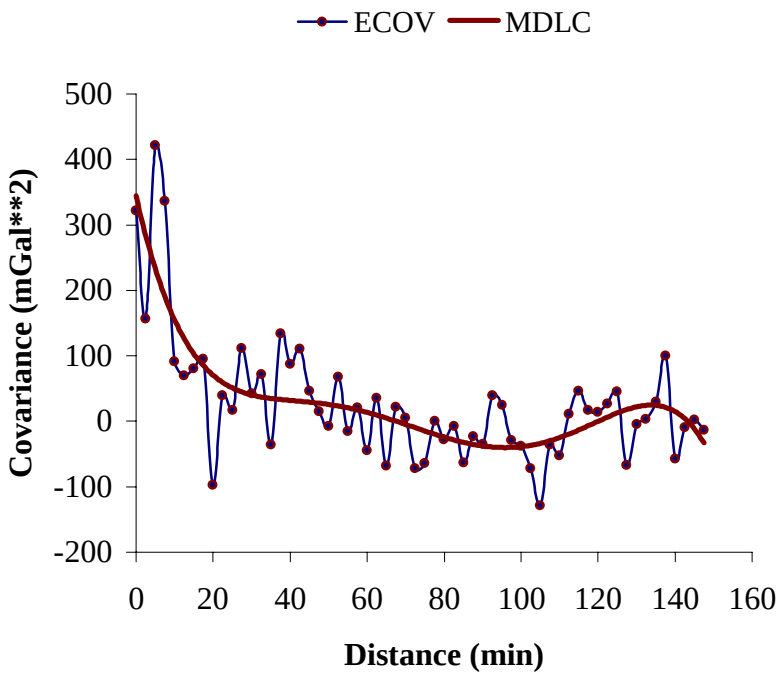

Figure 6.8: GPS/leveling geoid error covariance function for a mountainous area

Table 6.1: Parameters for external geoid error covariance function model

Test Area	Polynomial Model Parameters				
	a_o	a_1	a_2	a_3	a_4
Mountainous	344.35	-26.34	0.86	-0.01	0.0001
Flat	302.12	-38.74	1.35	-0.02	0.0001

The large discrepancy between the internal and external geoid error variances (Figures 6.4, 6.7 and 6.8) in the two selected areas could be partially attributed to errors that are not accounted for in the estimation of the external geoid error. Such errors include those in the

leveling and GPS data, as well as datum biases (Kotsakis and Sideris, 1999). As expected, the variance of geoid error covariance function for the western area is higher compared to the corresponding value for the eastern area.

The reliability of the external GPS/levelling derived geoid errors depends on how accurate the GPS and orthometric observations are. Thus it should be use as standard to test the accuracy of the gravimetric geoid if the accuracy of the GPS and heights are know. The internal propagated geoid errors on the other hand, provides useful information on the relation between the gravity anomaly errors, the GM errors and the computed geoid undulations. The reliability of the internal errors depends on how accurate the source data errors are know. This type of error should be used in gravity field prediction with geoid undulations as input data.

CHAPTER 7

7.1 SUMMARY

Gravity field data in areas with different topographic features have been analyzed to derive characteristics of the gravity field signal and errors for local areas. Firstly, the effect of truncating the spherical harmonic expansion of the GM coefficients in favour of using lager cap size for Stokes's integral solution is investigated in order to derive the appropriate combination techniques for the two data types. In addition, the effect of using lateral density variations for terrain correction computation and geoid estimation in the Mountainous Mountains is also investigated.

Secondly, estimates of local gravity empirical covariance functions for mountainous, flat and mountainous areas of Canada are derived using space domain and spectral methods. Models for the empirical covariance functions are derived for all the areas by fitting some analytical function to the space domain empirical covariance values. In addition, the sampling density of gravity data required for a centimetre to decimetre accuracy level of the geoid is estimated separately for the flat and mountainous areas.

Finally, estimates of gravity error covariance function for mountainous and flat areas are derived and compared. Geoid errors propagated form both gravity data and geopotential model coefficient errors are also estimated; the results are then compared to the external geoid error derived from GPS/levelling data.

7.2 CONCLUSION

From the analysis and results presented in this report, the following can be concluded:

A. The covariance functions for areas in Canada with similar topographic and geophysical features are rather stationary, while the covariance functions for areas with different topography vary widely with the topography. The results of both the space domain and spectral method of empirical covariance determination are similar in areas with flat terrain. The result of the two methods is very different for areas with rough topography. The difference is attributed to the smoothing effect introduced by the gridding procedure, and radial averaging used in the spectral method, as well as the distance averaging used in the spatial method. The smoothing effect depends on the roughness of the topography and the distribution of the data points in the local area.

B. The decay of the geoid spectrum in medium and high frequencies is not constant, and it also varies with the topographic height differences. For certain areas in Canada, the rate of decay is different from the decay implied by the Kaula rule (decay rate = 3) in medium and high frequencies. Between 180 and 3030 harmonic degree the rate of decay is about 3.2 while for frequencies above harmonic degree of 3030, the geoid spectrum decay even faster at about 4.6.

C. The data resolution required for centimetre to decimetre accuracy level of geoid estimation varies between the flat and mountainous areas. In the mountainous area, a 1 cm geoid estimate will require grid data with 1′ spacing while in the flat areas, a 5′ grid data is required to achieve the same level of accuracy.

D. The difference between terrain corrections estimated with constant and varying density values is correlated with the topography of the local area. The computation of terrain corrections with actual density values using the prism mass model for the topography is required in the mountainous areas if the centimetre geoid is to be achieved in these areas.

E. The best achivable accuracy of the geoid estimated by the combination of a GM with the Stokes's integral can be obtained if the cap size used in the Stokes integral is not less than 10°×10° and the harmonic degree of expansion not less than 200 with the EGM96. Using larger areas and higher degrees of expansion does not neccessarily improve the geoid accuracy.

F. The gravity error covariance function for both flat and mountainous areas of Canada can be modeled with a function of the form $E_{\Delta g}(\psi_{1:2}) = a_o e^{-a_1^2 \psi_{1:2}}$, for $\psi_{1:2}$ in degrees, and so can the corresponding geoid error covariance function be modeled with the function $E_N(\psi_{1:2}^2) = a_o e^{-a_1^2 \psi_{1:2}^2}$. In both cases, a_o represents the variance of the error covariance function.

G. The spectrum of the geoid error is mainly dominated by errors from the geopotential model, consequently, for both flat and mountainous areas, the combined geoid errors from GM coefficients and gravity data are quite similar. The results of the internal propagated and external geoid errors disagree in both the flat and the mountainous areas tested; estimates of the total geoid error are higher in the mountainous areas when compared to those of the flat areas.

7.3 RECOMMENDATIONS AND FUTURE PLANS

The following recommendations are proposed for further research:

1) A new geoid model based on the results of the findings herein should be computed for Canada using, e.g., a 10° ×10° cap size for Stokes's integration, variable topographic density for rigorous modelling of the terrain correction and geoid indirect effect, and new denser gravity anomalies and digital topographic heights. The new geoid model should be compared to previous geoid models for Canada, as well as global models to assess the improvement in the geoid especially in the mountainous areas of Canada.

2) To derive gravimetric geoid in mountainous areas with an absolute accuracy of 5 cm or better, both the gravity anomalies and the digital topographic heights with 1′ resolution are require. Therefore, the present gravity data have to be improved in terms of data coverage, density and precision.

3) As it has been pointed out in chapters 4 and 6 of this thesis, gravity field signal and error covariance functions over Canada are not constant; it vary from one area to the other. Further studies on the effect of using different signal and error covariance functions for gravity field prediction in areas with different topographic features should be done. In addition, covariance models that would provide optimal results for gravity field approximation with heterogeneous data set should be derived separately for the flat, mountainous and marine areas.

4) The internal geoid error derived from the propagation of both the gravity anomaly errors and the geopotential harmonic coefficients (EGM96), provides useful information on the relation between the gravity anomaly errors, the GM errors and the

computed geoid undulations. Numerical investigation to derive internal geoid undulation errors for all in Canada should be done. The relation between the internal errors estimates and the external accuracy estimation that are obtained by comparing gravimetric geoid with GPS/levelling derived geoid on benchmarks should also be investigated for all areas in Canada.

5) Error covariance models for the geoid indirect effect should be derived and the effect on the total geoid error should be evaluated especially in the mountainous areas.

6) In order to provide a reasonable external standard for evaluating the accuracy of gravimetric geoid undulation, it is necessary to investigate the quality (accuracy) of the GPS and levelling observations that are used in estimating the external geoid accuracy. This is more important in the mountainous areas, where it is believed that the accuracy of the orthometric heights is poorer when compared to those of the flat areas.

REFERENCES

Balmino, G., B. Moynot, M. Sarrailh, and N. Vales. 1987. Free air gravity anomalies over the ocean from SEASAT and GEOS-3 altimetry data. *EOS Trans. AGU*, Vol. 68, pp. 17-19.

Barzaghi, R., A. Fermi, S. Tarantola, and F. Sansò. 1993. Spectral techniques in inverse Stokes and overdetermined problems. *Surveys in Geophysics*, Vol. 14, No. 4-5.

Bendat, J.S. and A.G. Piersol. 1986. *Random data: Analysis and measurement procedures*, Second edition, John Wiley and Sons, New York.

Bendat, J.S. and A.G. Piersol. 1980. *Engineering Applications of Correlation and Spectral Analysis.* John Wiley and Sons, New York.

Blais J.A.R. 1982. Synthesis of Kriging Estimation Methods. *Manuscripta Geodetica* Vol. 7, pp. 325 - 352.

Bottoni, G.P. and R. Barzaghi. 1993. Fast collocation. *Bulletin Géodésique*, Vol. 67, No. 2, pp. 119-126.

Bracewell, R.N. 1986. *The Fourier transform and its applications*, Second edition, revised. McGraw-Hill, New York.

Esan, O. and M. G. Sideris. 1999. On the Role of the GM, Error Propagation, and Optimal Combination of GM with Local Gravity Data in Precise Geoid Determination. Report Submitted to Geodetic Survey Canada.

Forsberg, R. 1984. Local covariance functions and density distributions. OSU Report No. 356, Department of Geodetic Science and Surveying, The Ohio State University.

Forsberg, R. 1987. A new covariance model for inertial gravimetry and gradiometry. *Journ. of Geophys. Res.*, Vol. 92, No. B2, pp. 1305-1310.

Forsberg, R. 1993. Impact of airborne gravimetry on geoid determination - the Greenland example. *Bul. International. Geoid Service*, No 2, pp. 32-43.

Forsberg, R. and S. Kenyon. 1995. Downward continuation of airborne gravity data. *Proc. of IAG Symposium G4, IUGG XXI General Assembly,* Boulder, Colorado, July 2-14, 1995. pp. 73-80.

Haagmans, R. E. de Min and M. van Gelderen, 1992. Evaluation of Stokes' and other integrals using 1D-FFT and a comparison with existing methods. Paper submitted to *Manuscripta Geodetica*.

Hammer, S. 1983. Airborne gravity is here! *Geophysics*, Vol. 48, No. 2, pp. 213-223.

Heiskanen, W. A. and H. Moritz. 1967. *Physical geodesy.* W. H. Freeman and Company. San Francisco.

Kaula, W.M., *Theory of Satellite Geodesy*, Blaisdell Publishing Co., 1966.

Kotsakis, C. and M. G. Sideris. 1998. Study of the gravity field spectrum in Canada in view of cm-Geoid Determination. Paper presented at the Second Joint Meeting of the Internaional Gravity Commission and the Geoid Commission Trieste, Italy, Sept. 7-12, 1998. Also submitted to *Journ. of Geodesy.*

Kotsakis, C. and M. G. Sideris. 1999. On the Adjustment of Combined GPS/Levelling/Geoid Networks. Paper presented at the IV Hofine-Marusi Symposium on Mathematical Geodesy Trento, Italy, Sept. 14 - 17 1998.

Li, Y.C. 1993. Optimized spectral geoid determination. UCGE Report No. 20050, Department of Geomatics Engineering, The University of Calgary, Calgary, Alberta.

Li, J. and M.G. Sideris. 1995. Marine gravity and geoid determination by optimal combination of satellite altimetry and shipborne gravimetry data. Paper presented at the XXI IUGG General Assembly, July 2-14, Boulder, Colorado. Also submitted to the *Journal of Geodesy*.

Li, Y.C. and M.G. Sideris. 1994. Minimization and estimation of geoid undulation errors. *Bulletin Géodésique*, Vol. 68, pp. 201-219.

Moritz, H. 1980. *Advanced Physical Geodesy*. H. Wichmann verlag, Karlsruhe, Germany.

Pavlis, N. K. 1997. Development and applications of geopotential models. Prepared for the Second international school for the determination and use of the geoid, Rio de Janeiro, Brazil.

Rapp, R. H., Y. M. Wang and N. K. Pavis. 1991. The Ohio State 1991 geopotential and sea surface topography harmonic coefficient models. OSU Report No. 410, Department of Geodetic Science and Surveying, The Ohio State University, Ohio, USA.

Rapp, R. H. and N. K. Pavlis, 1990. The development and analysis of geopotential coefficient models to spherical harmonic degree 360. *Journ. of Geophys. Res.* Vol. 95, No. B13, pp. 21885 - 21911.

Schwarz, K. P. 1984. Data types and their spectral properties, Proceedings of Local Gravity Field Approximation. Beijing, China, August 21 - September 4.

Schwarz, K.P. 1987. Geoid profiles from an integration of GPS satellite and inertia data. *Bollettino Di Geodesia e Scienze Affini*. Anno XLVI, N. 2, pp. 117-131. Presented at the International Symposium on the Definition of the Geoid, Florence, Italy, May 26-30, 1986.

Schwarz, K. P. and Y.C. Li. 1995. What can airborne gravimetry contribute to geoid determination? *Proc. of IAG Symposium G4, IUGG XXI General Assembly*, Boulder, Colorado, July 2-14, 1995. pp. 143-152.

Schwarz, K. P. and M.G. Sideris. 1985. Precise geoid heights and their use in GPS interferometry. GSD Report NO. 85-004. Geodetic Survey Canada.

Schwarz, K. P., Sideris M. G. and R. Forsberg. 1989. The use of FFT techniques in physical geodesy. *Geophys. Journal Inter.*, Vol. 100, pp. 485-514.

Schwarz, K. P. and M. Wei. 1994. Some unsolved problems in airborne gravimetry. Paper presented at the Symposium *'Gravity and Geoid'*, Graz, Austria, September 11-17.

Schwarz, K. P. and M. Wei. 1992. *Inertia surveying and INS/GPS integration*. Lecture Notes, Department of Geomatics Engineering, The University of Calgary, Calgary, Alberta, Canada.

Seeber, G. 1993. *Satellite Geodesy*. Walter de Gruyter, Berlin, New York.

Sideris, M.G. 1987. On the application of spectral techniques to the gravimetric problem. *Proc. of the XIX IUGG General Assembly*, Tome II, Vancouver, BC, August 9-22, pp. 428-442.

Sideris, M.G. 1995. On the use of heterogeneous noisy data in spectral gravity field modelling methods. Invited paper, presented at the XXII IUGG General Assembly, Colorado, July 2-14, 1995.

Sideris , M.G. and B.B. She, (1994): A new, high-resolution geoid for Canada and part of the U.S. by the 1D FFT method. *Bulletin Geodesique* Vol. 69, No 2, pp. 92-108.

Sideris, M.G. and K. P. Schwarz. 1986. The use of GPS and DOPPLER heights in NAVD. Paper presented at the Fourth International Geodetic Symposium on Satellite Positioning, Austin, Texas, April 28-May2, 1986.

Sideris, M.G. and K. P. Schwarz. 1987. Improvement of the medium and short features of geopotential solutions by local gravity data. *Bollettino Di Geodesia e Scienze Affini*. Anno XLVI, N. 3, pp. 206-221.

Sideris, M.G. and Y. Li. 1992. Improved geoid determination for leveling by GPS. In Proc. of the sixth Int. Geodetic Symposium on Satellite Positioning Vol. II, pp. 873 - 882, Columbus, Ohio, March 17- 20.

Sjoberg, L. E. 1987. Progress in global gravity field approximation, Contributions to geodetic theory and methodology. XIX general meeting of the IUGG, Vancouver, BC, Canada, August 2-22.

Tscherning, C. C. 1975. Covariance expression for second and lower order derivatives of the anomalous potential. Report of The Dep. of Geodetic Science No. 225, 1975.

Tscherning, C. C. 1984. Local approximation of the gravity potential by least-squares collocation. Proceedings of the international summer school on local gravity field approximation, Beijing, China, August 21 - September 4.

Tscherning, C. C. and R. H. Rapp. 1974. Closed covariance expression for gravity anomalies, geoid undulations and deflections of the vertical implied by anomaly degree- variance models. OSU Report No. 208, Department of Geodetic Science and Surveying, Ohio State University.

Veronneau M., (1996) Canadian Geoid Model GSD95 and its precision. *Geodetic Survey Division Canada, internal report.*

Weber G. and H. G. Wenzel. 1983. Error covariance functions of sea gravity data and implications for geoid determination. *Marine Geodesy.* Vol. 7, Number 1-4

Wu, L. and M.G. Sideris. 1995. Using multiple input-single output system relationships in post processing of airborne gravity vector data. *Proc. of IAG Symposium G4, IUGG XXI General Assembly,* Boulder, Colorado, July 2-14, 1995. pp. 87-94.

Zhang, C. and J. A. R Blais. 1995. Comparison of methods for marine gravity determination from satellite altimetry data in the Labrador Sea. *Bulletin Géodésique*, Vol. 69, pp 173-180.

Zhang, C. and J. A. R Blais. 1993. Recovery of gravity distubances from satellite altimetry by FFT techniques: a synthetic study. *Manuscripta Geodaetica*, Vol. 18, pp. 158-170.

Zhang, C. and M. G. Sideris. 1995. Gravity disturbances from GEOSAT data and forward geopotential models in the Labrador Sea. *IAG Symposia 113*, convened and editted by Sunkel, H. and I. Marson, Springer, pp. 317-328.